Molecular Biology of the Cell
Vol. 19, 2311–2327, May 2008

Multiplexed Dendritic Targeting of α Calcium Calmodulin-dependent Protein Kinase II, Neurogranin, and Activity-regulated Cytoskeleton-associated Protein RNAs by the A2 Pathway

Yuanzheng Gao,*† Vedakumar Tatavarty,*† George Korza,‡ Mikhail K. Levin,‡§ and John H. Carson‡§

*Neuroscience Program, ‡Department of Molecular Microbial and Structural Biology; §Richard Berlin Center for Cell Analysis and Modeling, University of Connecticut Health Center, Farmington CT 06030

Submitted September 18, 2007; Revised January 2, 2008; Accepted February 19, 2008
Monitoring Editor: Karsten Weis

In neurons, many different RNAs are targeted to dendrites where local expression of the encoded proteins mediates synaptic plasticity during learning and memory. It is not known whether each RNA follows a separate trafficking pathway or whether multiple RNAs are targeted to dendrites by the same pathway. Here, we show that RNAs encoding α calcium calmodulin-dependent protein kinase II, neurogranin, and activity-regulated cytoskeleton-associated protein are coassembled into the same RNA granules and targeted to dendrites by the same *cis*/*trans*-determinants (heterogeneous nuclear ribonucleoprotein [hnRNP] A2 response element and hnRNP A2) that mediate dendritic targeting of myelin basic protein RNA by the A2 pathway in oligodendrocytes. Multiplexed dendritic targeting of different RNAs by the same pathway represents a new organizing principle for coordinating gene expression at the synapse.

INTRODUCTION

In neurons, genetic information is transmitted from nucleus to synapse in the form of RNA molecules that are translated locally in dendrites to provide proteins required for synapse formation and plasticity. In situ hybridization studies of brain have identified many dendritically localized RNAs (Lein *et al*., 2007). It is not known whether each of these RNAs follows a separate trafficking pathway or whether different RNAs are targeted to dendrites by the same pathway. In telecommunications, a process called multiplexing is used to combine multiple messages into a composite signal for transmission by a single carrier. Here, we show that a similar process of multiplexing is used in neurons for transmission of multiple, different RNAs from nucleus to synapse by the A2 pathway.

The A2 pathway was first characterized in oligodendrocytes as a pathway for targeting myelin basic protein (MBP) RNA to the myelin compartment (Ainger *et al*., 1993). The same pathway has been shown to target exogenous heterologous RNAs to dendrites in neurons, but endogenous neuronal RNA substrates for the A2 pathway have not been identified experimentally (Shan *et al*., 2003). The fundamental trafficking intermediate in the A2 pathway is the RNA granule (Ainger *et al*., 1993), a composite structure containing multiple RNA molecules, cognate RNA binding proteins (Mouland *et al*., 2001), components of the translational machinery (Barbarese *et al*., 1995), and molecular motors for transport along microtubules (Carson *et al*., 1997). Targeting by the A2 pathway requires a characteristic 11-nucleotide *cis*-acting RNA sequence, the hnRNP A2 response element (A2RE) (Ainger *et al*., 1997), that is recognized by a cognate *trans*-acting factor, heterogeneous nuclear ribonucleoprotein (hnRNP) A2 (Hoek *et al*., 1998). MBP RNA contains two partially overlapping A2RE sequences (GCCAAGGAGCC and GCCAGAGAGCC) (Munro *et al*., 1999), and A2RE sequences have also been identified in the *gag* and *vpr* genes of human immunodeficiency virus (HIV) (Mouland *et al*., 2001). A2RE-like sequences have been noted in dendritically localized neuronal RNAs protein kinase Mζ (PKMζ) (Muslimov *et al*., 2004) and BC1 (Muslimov *et al*., 2006), but it is not known whether these RNAs are targeted by the A2 pathway. Because polymorphisms at several positions in the A2RE sequence are compatible with hnRNP A2 binding and dendritic targeting (Munro *et al*., 1999) sequence homology alone is not sufficient to identify functional A2RE sequences. In this study, functional A2RE sequences in α calcium calmodulin-dependent protein kinase II (αCaMKII), neurogranin (NG), and activity-regulated cytoskeleton-associated protein (ARC) RNAs are identified by three criteria: significant sequence similarity to one of the A2RE sequences in MBP RNA, high-affinity binding to hnRNP A2, and necessary and sufficient for dendritic targeting in microinjected neurons.

This article was published online ahead of print in *MBC in Press* (http://www.molbiolcell.org/cgi/doi/10.1091/mbc.E07–09–0914) on February 27, 2008.

† These authors contributed equally to this work.

Address correspondence to: John H. Carson (jcarson@nso2.uchc.edu).

Abbreviations used: A2RE, hnRNP A2 response element; ARC, activity-regulated cytoskeleton-associated protein; αCaMKII, calcium calmodulin-dependent protein kinase IIα; demux, demultiplexer; FBS, fetal bovine serum; FCCS, fluorescent cross-correlation spectroscopy; FISH, fluorescent *in situ* hybridization; HBSS, Hank's balanced salt solution; hnRNP, heterogeneous nuclear ribonucleoprotein; mux, multiplexer; NG, neurogranin; PKMζ, protein kinase Mζ; SPR, surface plasmon resonance.

αCaMKII, NG, ARC, and PKMζ RNAs are all dendritically localized in hippocampal neurons where the encoded proteins regulate synaptic activity during learning and memory. NG and αCaMKII are expressed constitutively at the synapse (Benson *et al*., 1992; Guadano-Ferraz *et al*., 2005) and have opposing effects on synaptic sensitivity. NG sequesters calmodulin (Zhabotinsky *et al*., 2006), preventing it from activating αCaMKII. When the synapse is activated, calmodulin dissociates from NG and binds to αCaMKII, which phosphorylates α-amino-3-hydroxy-5-methyl-4-isoxazolepropionic acid (AMPA) receptors (Lisman *et al*., 2002; Rongo, 2002). ARC and PKMζ are induced by synaptic activity (Lyford *et al*., 1995; Ling *et al*., 2006), and they have opposing effects on synaptic scaling. ARC stimulates endocytosis of AMPA receptors (Rial Verde *et al*., 2006; Shepherd *et al*., 2006), whereas PKMζ activity increases the number of AMPA receptors at synapses (Ling *et al*., 2006).

Several different *cis*-acting dendritic localization elements have been reported in αCaMKII, NG, ARC and PKMζ RNAs. Mayford found that dendritic localization of αCaMKII RNA requires sequences in the 3′-untranslated region (UTR) (Mayford *et al*., 1996). Mori identified a 94-nt element near the beginning of the 3′UTR of rat αCaMKII RNA and a similar element in the 3′UTR of NG RNA that are sufficient for dendritic localization of heterologous RNAs in transfected neurons (Mori *et al*., 2000). Blichenberg *et al*. (2001) identified a 1200-nt region in the 3′UTR of rat αCaMKII RNA, distinct from the element identified by Mori *et al*. (2000), that is sufficient for dendritic localization. Miller *et al*. (2002) showed that the element identified by Mori *et al*. (2000) is not sufficient for dendritic localization of mouse αCaMKII RNA in transgenic mouse brain. Huang *et al*. (2003) reported that the cytoplasmic polyadenylation element (CPE) near the 3′ end of mouse αCaMKII RNA is sufficient for dendritic localization of heterologous RNA in transfected neurons (Huang *et al*., 2003). Kobayashi identified a *cis*-acting element in the 3′UTR of ARC RNA required for dendritic localization in neurons (Kobayashi *et al*., 2005). Muslimov *et al*. (2004) identified two dendritic localization elements in PKMζ RNA: one element at the interface between the 5′UTR and the open reading frame (ORF), and the other element in the 3′UTR. The various dendritic localization elements identified in αCaMKII, NG, ARC, and PKMζ RNAs have no obvious similarities.

Identification of *cis*/*trans*-targeting determinants for different RNAs is complicated, because the subcellular distribution of each RNA can be affected by multiple different cellular processes in both nucleus (splicing, RNP assembly) (Farina and Singer, 2002; Hachet and Ephrussi, 2004; Czaplinski and Singer, 2006; Giorgi and Moore, 2007) and cytoplasm (granule assembly, transport, localization, and degradation). Each process can be mediated by distinct *cis*/*trans*-determinants, so that different RNAs may have the same determinants for some processes but different determinants for other processes. To identify *cis*/*trans*-determinants for one particular process the experimental assay system must be designed to focus on that process and to minimize confounding effects of other processes. This study uses a microinjection assay designed to analyze dendritic targeting in the cytoplasm. To avoid potential effects of nuclear processes, fluorescent RNA is microinjected into the cytoplasm rather than into the nucleus. To minimize potential effects of translation, injected RNAs are not capped or polyadenylated and also contain fluorescent nucleotides, all of which reduce translational efficiency of the injected RNA. To minimize potential effects of RNA degradation, injected RNA is analyzed soon after injection. The microinjection assay was used to identify *cis*-acting A2RE sequences in αCaMKII, NG, and ARC RNAs that are similar to the A2RE in MBP RNA, bind to hnRNP A2, mediate coassembly into the same granules, and are necessary and sufficient for dendritic targeting. This provides the basis for multiplexed dendritic targeting of these RNAs in neurons.

MATERIALS AND METHODS

Primary Hippocampal Neuron Culture

Hippocampi dissected from E18 Sprague-Dawley rats were incubated in trypsin Hank's balanced salt solution. Cells were mechanically dissociated by trituration in 2 ml of Neurobasal medium with 10% fetal bovine serum (FBS) (Goslin and Banker, 1989). The dissociated cell suspension was allowed to settle for 3 min, after which the supernatant was transferred to a 15-ml tube and centrifuged at 1000 × *g* for 15 min. The cell pellet was resuspended in Neurobasal medium with 10% FBS, and plated at a density of ~600 cells/mm^2 on poly-L-lysine–coated dishes. After 3-h incubation at 37°C in 5% CO_2, the medium was changed to Neurobasal containing 1× B27 supplement, 1× antibiotics, 0.5 mM L-glutamine, and 25 μM L-glutamic acid. Every 4 d, half the medium was replaced with medium lacking L-glutamic acid.

Fluorescent RNA

Fluorescent RNAs were prepared by in vitro transcription of linearized template DNA in the presence of Alexa 488 or cyanine (Cy5)-conjugated uridine 5′-tiphosphate using AmpliScribe kit (Epicenter, Technologies, Madison, WI). RNAs were filtered through MicroBio-spin columns P-30 (Bio-Rad, Hercules, CA), precipitated in 5 M ammonium acetate, washed in 70% ethanol, and dissolved in water at a concentration of ~1 mg/ml. RNA integrity was assessed by electrophoresis on agarose-formaldehyde gel.

Plasmid PMM281containing full-length mouse αCaMKII cDNA (obtained from Dr. M. Mayford, University of California, Irvine) was linearized with EcoR1, BssHII, Hap1, or BamH1, and transcribed to make full-length or truncated mouse αCaMKII RNA. Plasmid pNE containing a truncated rat αCaMKII cDNA, including a portion of the ORF and the complete 3′UTR (obtained from Dr. S. Kindler, University Hospital Hamburg-Eppendorf, Germany) was digested with Not1 to excise the 3.5-kb cDNA fragment, which was recloned into the Not1 site of pBluescript II SK(+) (pBSII) vector. The resulting plasmid containing the A2RE sequence (1314 5′-GGCAAGGAGAG-3′ 1324) was linearized with Sac1 and transcribed to make rat αCaMKII RNA. Full-length NG cDNA (obtained from Dr. J. B. Watson, David Geffen School of Medicine at UCLA, Los Angeles, CA) was amplified by polymerase chain reaction (PCR) and recloned into pBSII between KpnI and XbaI sites. Plasmid DNA was linearized with XbaI or Tth111I and transcribed to make full-length and truncated NG RNA. Plasmid pBSII containing full-length ARC cDNA (obtained from Dr. Paul Worley, Johns Hopkins University, Baltimore, MD) was linearized with Xho1, PvuII, or XmnI and transcribed to make full-length and truncated ARC RNA. Plasmid PNKT7 containing green fluorescent protein (GFP) cDNA with or without the MBP A2RE insert was linearized with BsaW1 and transcribed in vitro to make A2RE GFP RNA and GFP RNA.

The A2RE in mouse αCaMKII RNA (2086 5′-GCCAGTGAGCC-3′ 2096) was deleted by site-directed mutagenesis by using primers (5′-GAGAGAGGAGCCAACAGGAACTGCTGCTC-3′ and 5′-GAGCAGCAGTTCCTGTTGGCTCCTCTCTC-3′). The A2RE in rat αCaMKII RNA (1314 5′-GGCAAGGAGAG-3′ 1324) was deleted by site-directed mutagenesis by using primers (5′-GCATTTGGCAGGAAGTAAGAGGGCGAGCTG-3′ and 5′-CAGCTCGCCCTCTTACTTCCTGCCAAATGC-3′). The A2RE in NG RNA (1169 5′-CCCUGAGAGCA-3′ 1179) was deleted by site-directed mutagenesis by using primers (5′-GAGAGCGGAGGGGCCGCGTTCTCAAGAGA-3′ and 5′-TCTCTT GAGAACGCGGCCCCTCCCGCTCTC-3′). The A2RE in ARC RNA (1162 5′-GCTGA GGAGGA-3′ 1172) was deleted by site-directed mutagenesis using primers (5′-GACAC TGTATGTGGACGGAGATCATTCAGTATGTGG-3′ and 5′-CCACATACTGAATGATCTCCGTCCACATACAGTGTC-3′). *Pfu* polymerase was used for extension reaction. Nonmutated parental DNA plasmid was digested with Dpn1. Nicks in the mutated plasmid were repaired in AL1-blue supercompetent cells after transformation. Desired deletions were confirmed by sequencing.

A2REs from αCaMKII, NG, and ARC RNAs were inserted into the 3′UTR of GFP by digesting PNKT7 with Sac1 and ligating the linearized plasmid with annealed oligonucleotides containing A2REs with Sac1 linkers (5′-GCCAGTGAGCCAGCT-3′ and 5′-GGCTCACTGGCAGCT-3′ for mouse αCaMKII A2RE, 5′-GGCAAGGAGAGAGCT-3′ and 5′-CTCTCCTTGCCAGCT-3′ for rat αCaMKII A2RE, 5′-CCCTGAGAGCAAGCT-3′ and 5′-TGCTCTCAGGGAAGCT-3′ for NG A2RE, and 5′-GCTGAGGAGGAAGCT-3′ and 5′-TCCTCCTCAGCAGCT-3′ for ARC A2RE). Insertion of A2REs was confirmed by sequencing. Plasmid DNA was digested with BsaW1 and transcribed in vitro to prepare GFP RNA containing A2REs from αCaMKII, NG, or ARC RNA.

Microinjection

Fluorescent RNAs were microinjected into the perikarya of hippocampal neurons in culture using the same procedure as described previously for

oligodendrocytes (Ainger *et al*., 1993). Injection needles were prepared from thin-walled borosilicate glass capillaries (with filament) using a Flaming/Brown pipet puller (Sutter, Novato, CA). RNAs were filtered through 0.2-μm filters before injection to remove aggregates and particulate matter. The concentration of RNA in the needle was 0.5–1 mg/ml. Within this concentration range, dendritic targeting was not affected by concentration and the RNA did not aggregate in the injection needle. Microinjection was performed with an Eppendorf pressure injection system with the Z-limit positioned several micrometers above the substratum and an injection time of 0.5 s. After injection cells were incubated at 37°C for 30–45 min to allow time for transport of injected RNA to dendrites after which injected cells were either imaged directly or fixed for immunostaining. In a typical experiment, ~100 cells were microinjected and the yield of injected cells that were useful for imaging was ~50 cells. The yield of cells could be affected by a number of variables, including: density and age of the cell culture, size and shape of the injection needle, holding pressure and injection pressure settings on the microinjector, Z-limit setting on the micromanipulator, and concentration and purity of the RNA in the needle. Cells that were damaged during the microinjection process were readily identified during imaging by lack of diffuse fluorescence in the perikaryon or blebbing of the cell membrane. In some experiments, antibodies to hnRNP A2 or GFP (~1 mg/ml) were coinjected with fluorescent RNAs (1:1, vol/vol). Mouse monoclonal antibody (mAb) to hnRNP A2 (clone EF67) recognizing an epitope corresponding to the C-terminal 18 residues of the protein was obtained from Dr. W. Rigby (Dartmouth College, Lebanon, NH). mAb to recombinant GFP was obtained from Clontech (Mountain View, CA).

Immunocytochemistry

Hippocampal neurons were fixed in 4% paraformaldehyde (PFA) in phosphate-buffered saline (PBS) for 15 min at room temperature (RT), washed three times in PBS, incubated in 10% (vol/vol) donkey serum in PBS with 0.2% Triton X-100 for 20 min, washed three times in PBS, and incubated with primary antibody diluted in 10% donkey serum for 1 h at RT. Mouse anti-hnRNP A2 mAb EF67 (obtained from Dr. W. Rigby) was used at 1:400 dilution. Cells were washed three times in PBS before adding secondary antibody (1:400 Alexa 647 conjugated; Invitrogen) at RT for 1 h. Cells were washed three times in PBS before adding mounting medium. Immunofluorescence was imaged by confocal microscopy (Zeiss 510 with 63×, 1.4 numerical aperture [NA] objective).

Fluorescent In Situ Hybridization (FISH) and Immunocytochemistry

Hippocampal neurons were fixed in 4% PFA in PBS for 15 min at RT, and then washed three times in PBS (diethyl pyrocarbonate treated) at RT. Cells were permeabilized in 70% ethanol at 4°C overnight. For hybridization, cells were washed in PBS and incubated at 37°C in a moisturized chamber for 16 h with 50 ng/ml digoxigenin (DIG)-labeled probes (antisense 5′-GGAAGTGGACGATCTGCCATTTTCCATCCCTGCGGTGCCAGACACGGG-3′, sense 5′-CCCGTGTCTGGCACCGCAGGGATGGAAAATGGCAGATCGTCCACTTCC-3′ for CaMKII RNA; antisense 5′-CCACTCTTTATCTTCTTCCTCGCCATGTGGCCCCGAAAACTCGCCTGG-3′, sense 5′-CCAGGCGAGTTTTCGGGGCCACATGGCGAGGAAGAAGATAAAGAGTGG-3′ for NG RNA; antisense 5′-TGCCCACCGACCTGTGCAACCCTTTCAGCTCTCGCTCCACCTGCTTGG-3′, sense 5′CCAAGCAGGTGGAGCGAGAGCTGAAAGGGTTGCACACAGGTCGGTGGGCA3′ for ARC RNA; antisense 5′-GCCGATCCACACGGAGTACTTGCGCTCAGGAGGAGCAATGATCTTGAT-3′, sense 5′-ATCAAGATCATTGCTCCTCCTGAGCGCAAGTACTCCGTGTGGATC GGC-3′ for β-actin RNA) diluted in hybridization buffer (10 mg/ml poly(A), 10 mg/ml single-stranded [ssDNA], 10 mg/ml tRNA, 1 mM dithiothreitol, 50× Denhart's, SSC, dextran sulfate, and deionized formamide). After hybridization, cells were washed two times in 2× SSC with 50% formamide for 15 min at 55°C, 2 times in 1× SSC with 50% formamide for 15 min at 55°C, and 1 time in 1× SSC with 50% formamide for 10 min at RT and incubated with 0.2% BSA in PBS for 10 min at RT before addition of primary antibody. Cells were incubated with primary antibodies (sheep anti-DIG polyclonal antibody [1:1000 dilution from 200 μg/ml; Roche Diagnostics, Indianapolis, IN] and mouse anti-hnRNP A2 mAb [1:400 dilution] for 1 h at RT and washed three times in PBS. Cells were incubated with secondary antibodies, donkey anti sheep immunoglobulin (Ig)G conjugated with Alexa 594 (1:800; Invitrogen), donkey anti mouse IgG conjugated with Alexa 488 (1:400) for 40 min at RT and washed in PBS with 8% formamide (vol/vol) for 30 min at RT. Cells were mounted in anti-fade reagent (Invitrogen). To detect ARC RNA cells were incubated with 0.3% hydrogen peroxide for 15 min, followed by detection with sheep anti-DIG-POD (1:400; Roche Diagnostics). Signal was amplified with tetramethylrhodamine-tyramide (Cy3 TSA-PLUS system; PerkinElmer Life and Analytical Sciences) for 10 min according to manufacturer's recommendations.

Image Analysis

Microinjected cells were scored as transport positive if RNA granules were detected at a distance greater than one cell diameter (~20 μm) from the perikaryon and distal to the first branch in at least two separate branches. The dynamic range of the microinjection assay is from ~20% positive for a nontransported RNA (GFP RNA) to ~70% positive for a transported RNA (GFP-A2RE RNA).

Differential interference contrast (DIC) images were subjected to processing to correct for imaging artifacts. To correct for uneven illumination a blurred version of the image was subtracted from the original image. To eliminate horizontal scan line artifacts, the image was subjected to filtering with a −1,1 kernel. To maximize contrast, grayscale levels were adjusted to maximize dynamic range. Fluorescent images were adjusted to maximize grayscale dynamic range.

Single granule ratiometric analysis of granule components was performed as described previously (Barbarese *et al*., 1995). Individual differentially labeled well-resolved granules were selected, and pixel intensities in the red and green channels were integrated and plotted as a two-dimensional scatter plot, where the *x*-axis is red intensity and *y*-axis is green intensity for each granule. To account for low level diffuse background fluorescence, granules with intensities <50 in either channel were considered to be deficient in the corresponding component.

Colocalization of granule components was also assessed by image correlation in spatial dimension (ICSD). To estimate the properties of RNA granules by image correlation, the correlation functions should be independent of cell shape, should exclude signal from extracellular regions of the image, and should be computed based only on the relevant image areas, which in case of RNA granules, include only dendrites. Image masks delineating dendritic processes were created based on DIC and fluorescence channels. Traditionally, correlation functions are computed in the Fourier domain, which is extremely efficient but requires a continuous rectangular image region with close-to-normal signal intensity distribution. Because of this requirement, Fourier domain image correlation cannot be used with confocal images of neurons. To overcome this limitation and to allow exclusion of regions not related to the dendrites of interest, we developed a program for ICSD by using a method similar to the program described previously (Barbarese *et al*., 1995) to calculate auto- and cross-correlation functions for a subset of pixels defined by an image mask delineating dendritic processes. Because the orientation of *x*- and *y*-axis of the image carry little biological significance, the cross-correlation function was computed isotropically as a function of radius (the distance between pairs of pixels). The value of cross-correlation at radius zero corresponds to Pearson's r, whereas the decay of the cross-correlation function over distance depends on the average dimensions of cellular structures responsible for colocalization of the labeled components. The cross-correlation data were analyzed by fitting into a two component Gaussian function.

Surface Plasmon Resonance

Surface plasmon resonance (SPR) measurements were performed using a Biacore T100 instrument. Ligand consisted of full-length recombinant hnRNP A2, prepared as described previously (Kosturko *et al*., 2006) immobilized by covalent carbodiimide coupling to a CM5 chip (Biacore, Uppsala, Sweden). The amount of protein immobilized on the chip was 5000 resonance units (RU), corresponding to 5 ng/mm^2. Analyte consisted of biotinylated oligoribonucleotides (purchased from Integrated DNA Technologies, Coralville, IA) representing A2RE sequences from rat MBP RNA (biotin-accGCCAAGGAGCC), mouse αCaMKII RNA (biotin-aacGCCAGUGAGCC), rat NG RNA (biotin-gcgCCCUGAGAGCA), rat ARC RNA (biotin-gacGCUGAGGAGGA), rat MBP A2RE antisense (biotin-uggCGGUUCCUCGG), rat αCaMKII RNA (biotin-uaaGGCAAGGAGAG), human αCaMKII RNA (biotin-gggGAGAAGGAGGG), and rat PKMζ RNA (biotin-gcaGCCAGAGAGGG). In each case, three additional 5′ flanking nucleotides were included as spacer between the A2RE sequence and the biotin moiety. Biotinylated oligoribonucleotides were bound to streptavidin (1:1 mol/mol) to enhance signal. Analyte in HEPES-buffered saline buffer (10 mM HEPES, 3 mM EDTA, 0.15 M NaCl, and 0.05% surfactant p20, pH 7.5) was injected at different concentrations (12.5, 25, 50, 100, and 200 nM) at a flow rate of 30 μl/min for 180 s, followed by HBS at 30 μl/min for 180 s. After each injection the surface of the chip was regenerated using 2.5 M NaCl at 100 μl/min for 20 s. Sensorgrams were globally fitted with Biacore T100 evaluation software. Because hnRNP A2 contains two independent RNA binding sites (Shan *et al*., 2000) SPR data were fitted with a heterogeneous two-site ligand binding model to determine k_{on}, k_{off}, and K_D values for two distinct binding sites in hnRNP A2. Control experiments with hnRNP E1 as ligand showed <100 RU binding at 200 nM for all analytes. Control experiments with streptavidin alone as analyte (no oligoribonucleotide) showed no detectable binding to hnRNP A2 ligand.

Fluorescence Cross-Correlation Spectroscopy

Fluorescence cross correlation spectroscopy (FCCS) measurements were performed using a Zeiss Confocor II with a 40× 1.2 NA objective. These experiments used an N-terminal fragment of hnRNP A2 (1–189) containing both RNA recognition motifs because of its superior solubility properties compared with full-length hnRNP A2. The N-terminal fragment of hnRNP A2 was conjugated with Alexa Fluor 488 succinimidyl ester and mixed with increasing concentrations of biotinylated oligoribonucleotides representing A2RE sequences from MBP, αCaMKII RNA, NG, or ARC RNA or a nonspe-

cific control RNA bound to Alexa Fluor 647-conjugated streptavidin. Total concentration of hnRNP A2 in each sample was determined from the amplitude of the autocorrelation function in the green channel. Total concentration of oligoribonucleotide was determined from the amplitude of the autocorrelation function in the red channel. Concentration of oligoribonucleotide bound to hnRNP A2 was determined from the amplitude of the cross-correlation function. Binding data over a range of oligoribonucleotide concentrations was fitted to a quadratic equation:

$$[A2::RNA] = \frac{K_D + RNA_{tot} + A2_{tot} - \sqrt{(K_D + RNA_{tot} + A2_{tot})^2 - 4RNA_{tot}A2_{tot}}}{2}$$

where K_D is the dissociation constant between hnRNP A2 and RNA, RNA_{tot} is total RNA concentration, and $A2_{tot}$ is total hnRNP A2 protein concentration. Because concentrations greater than 100 nM cannot be accurately measured by FCS, K_D values greater than 100 nM could not be determined by this method.

Electroconvulsive Shock (ECS)

ECS was administered to adult rats via saline soaked ear clip electrodes using the ECT Unit 57800-001 (Ugo Basile, Comerio, Italy). Square-wave pulses (100 Hz; 90 mA; 0.5 ms) were delivered to induce seizures. All animals had tonic convulsions with hind limb extension (n = 3). Control animals were sham treated, i.e., ear clips were put on, but no shock was administered (n = 3). Animals were killed by perfusion with 4% paraformaldehyde ~2.5 h after ECS. Brains were removed and kept overnight in 1% paraformaldehyde. Microtome sections were cut at 50 μm and stored in PBS until staining at 4°C. Staining was performed as described previously, with slight modifications (Birgbauer *et al*., 2004). In brief, floating sections were incubated with 0.3% hydrogen peroxide in PBS for 30 min followed by blocking for 2–3 h in blocking solution (1% bovine serum albumin [BSA], 10% horse serum, and 0.2% Triton X-100 in PBS) at RT. Monoclonal mouse anti-hnRNPA2 was used at 1:500 dilution overnight at 4°C in antibody incubation solution (1% BSA, 1% horse serum, and 0.2% Triton X-100 in PBS). Slices were washed three times for 30 min in 0.05% Triton X-100 in PBS, followed by incubation with anti mouse HRP (1:400) overnight at 4°C. Slices were washed again three times for 30 min in 0.05% Triton X-100 in PBS. Signal was amplified with tetramethylrhodamine-tyramide (Cy3 TSA-PLUS system; PerkinElmer Life and Analytical Sciences) for 15 min according to manufacturer's recommendations. Treatment of sections with peroxide immediately before detection with TSA reagent abolished >90% of the signal. Sections were mounted on slides and imaged with a Zeiss LSM confocal microscope. Three different control animals and three different ECS-treated animals were analyzed. The total number of granules and fluorescence intensities per granule were determined for three different regions of interest (100 μm^2).

RESULTS

αCaMKII, NG, and ARC RNAs Are Targeted to Dendrites in the Form of RNA Granules

Subcellular localization of endogenous αCaMKII, NG, and ARC RNAs in hippocampal neurons in culture was analyzed by in situ hybridization (Figure 1). Each of the RNAs was localized in discrete particulate structures in dendrites, indicating that they are targeted to dendrites in the form of RNA granules. The overall size of the particulate structures visualized by in situ hybridization is somewhat larger than fluorescent RNA granules visualized in live cells because of the tyramide amplification procedure used for detection. Variation in size and intensity among individual granules indicates that different granules contain different numbers of RNA molecules. The number of αCaMKII and NG RNA granules per cell is greater than the number of ARC RNA granules, which may reflect the fact that αCaMKII and NG are expressed constitutively in hippocampal neurons, whereas ARC is induced by synaptic activity. Sense probes gave much lower signal compared with antisense probes, indicating that signal detected by antisense probes is specific.

αCaMKII, NG, and ARC RNAs Contain A2RE Dendritic-targeting Elements

Dendritic targeting of exogenous αCaMKII, NG, and ARC RNAs was analyzed by microinjecting fluorescent RNA into hippocampal neurons and analyzing subcellular distribution of injected RNA by confocal microscopy. In most experiments, a small percentage of cells did not survive the microinjection process. These cells could be identified by the lack of diffuse fluorescence in the perikaryon, indicating that the injected RNA had leaked out of the cell. Several controls were performed to analyze long-term viability in cells that survived the initial injection (Supplemental Figure S1 and Supplemental Movie S1). Plasma membrane potential was measured in uninjected and injected neurons using tetramethyl rhodamine ester (a membrane potential dye) (Farkas *et al*., 1989). Average plasma membrane potential was comparable for uninjected cells (−50 ± 3 mV) and injected cells (−54 ± 3.7 mV), indicating that microinjection does not cause long-lasting cell depolarization. Cells were coinjected with an expression vector for hnRNP A2-mcherry fusion protein and FITC-labeled dextran as a cytoplasmic volume marker. Injected cells retained dextran for up to 96 h, indicating that the plasma membrane remains intact after microinjection. Injected cells also expressed hnRNP A2-mcherry fusion protein, indicating that microinjection does not interfere with macromolecular synthesis. Bidirectional movement of RNA granules in dendrites of injected cells was observed by time-lapse confocal microscopy (Supplemental Movie S1), indicating that injected cells retain molecular motor activity after injection. These experiments show that microinjection does not have long-term deleterious effects on neuronal cell viability. Similar controls were not repeated for each microinjection experiment, but since all microinjections were performed under comparable conditions, we believe the control results can be extrapolated to all microinjection experiments. Each injected cell was examined before image acquisition for signs of damage to the cell such as blebbing of the cell membrane. Degradation of the injected RNA, detected as accumulation of fluorescence in the nucleus was rarely observed. Cells with signs of damage or RNA degradation were not analyzed further.

Injected αCaMKII, NG, and ARC RNAs formed discrete granules that were targeted to dendrites in >70% of injected cells, whereas a control RNA (GFP RNA) was targeted to dendrites in <20% of injected cells (Figure 2), indicating that dendritic targeting of these RNAs can be analyzed by the microinjection assay with a dynamic range of 20–70%. In the small proportion of cells where αCaMKII, NG, and ARC RNAs were not targeted to dendrites the RNA may have been injected into a region of the cell that is not accessible to the RNA transport machinery. In the small proportion of cells where GFP RNA was targeted to dendrites the injected RNA may have been misassembled into dendritically targeted endogenous RNA granules.

The images in Figure 2 were collected with the confocal observation volume positioned close to the surface of the dish to visualize granules in dendrites adhering to the substratum. Images collected with the confocal volume positioned above the surface of the dish so that the optical section passed through the nucleus revealed that injected fluorescent RNA was excluded from the nucleus in most cells (data not shown). Because fluorescent products of RNA degradation can enter the nucleus this means that the injected RNA was not degraded during the course of the experiment. Furthermore, because RNA was injected directly into the cytoplasm and was not capped or polyadenylated, we can conclude that in this assay dendritic targeting of these RNAs does not require passage through the nucleus or translation in the cytoplasm.

The *cis*-acting dendritic-targeting elements in αCaMKII, NG, and ARC RNAs were identified by deletion analysis and site-directed mutagenesis of microinjected RNA (Figure

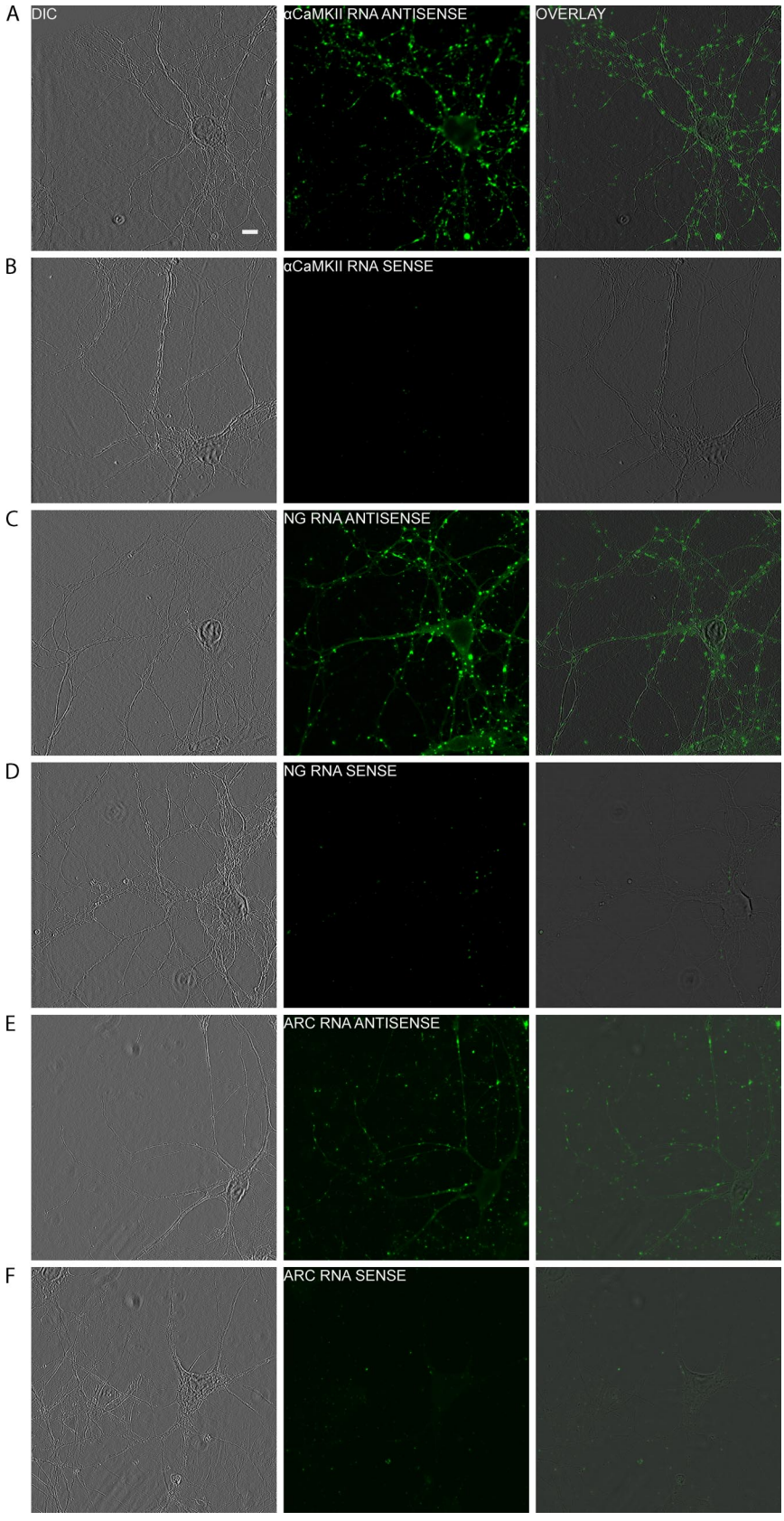

Figure 1. Subcellular distribution of endogenous αCaMKII, NG, and ARC RNAs in hippocampal neurons. Subcellular distribution of αCaMKII, NG, and ARC RNAs in hippocampal neurons was analyzed by in situ hybridization. Left panels show DIC images of representative cells. Center panels show in situ hybridization of the same cells performed with sense or antisense probes for αCaMKII, NG, and ARC RNAs. Right panels show merged DIC and in situ images. Bar, 10 μm.

2). Full-length mouse αCaMKII RNA (1-4888) was targeted to dendrites in 73% of injected cells. Truncation at positions 2997 or 2408 did not significantly affect dendritic targeting, indicating that the region downstream of position 2408,

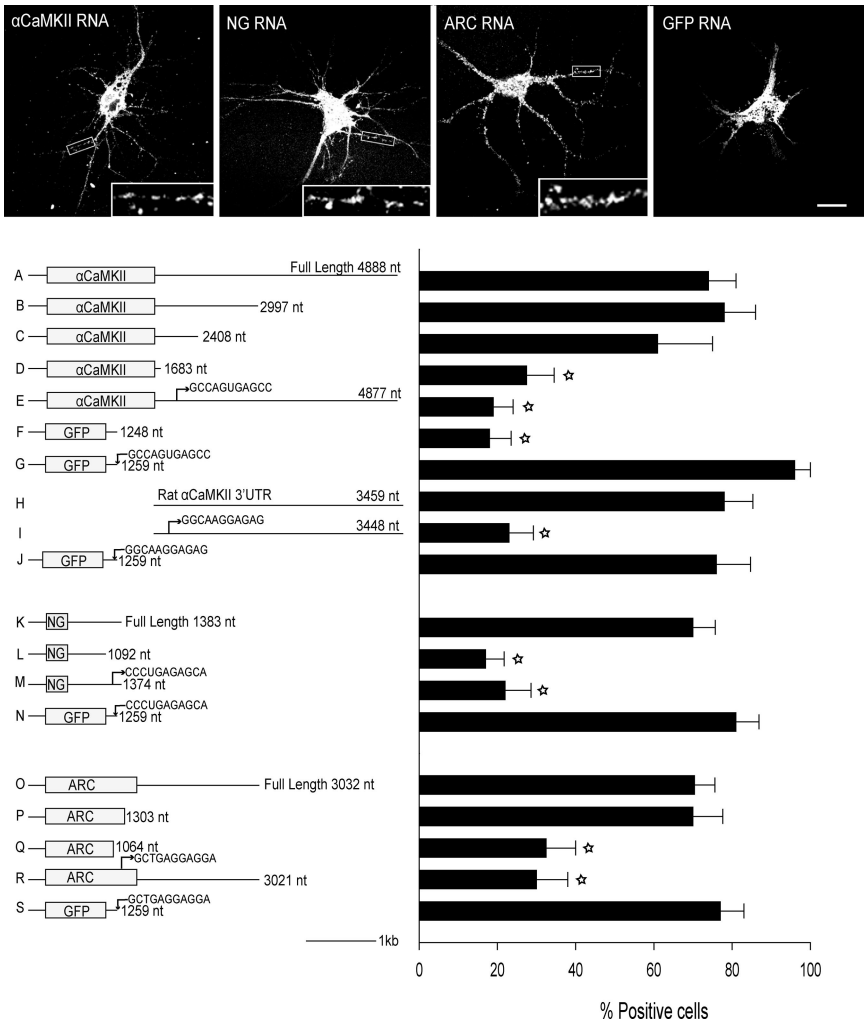

Figure 2. Identification of A2RE-like sequences in αCaMKII, NG, and ARC RNAs. Fluorescent RNAs, prepared as described in *Materials and Methods*, were microinjected into rat hippocampal neurons in culture. After ~30 min, the intracellular distribution of fluorescent RNA in the injected cells was analyzed by confocal microscopy. Top panels show representative cells injected with αCaMKII, NG, ARC, and GFP RNAs. Bar, 10 μm. Cells with RNA granules distal to the second branch in at least two dendrites were scored as transport positive. At least 50 cells were analyzed for each RNA. A–S show structural diagrams and percentage of transport positive cells for the various RNAs tested. Bar, 1 kb. The stars indicate dendritic targeting measurements that are different from wild type with >99.6% confidence by Fisher's exact test (Fisher, 1922).

including the previously identified CPEs (Huang *et al*., 2003), does not contain *cis*-acting elements necessary for dendritic targeting in this assay. Truncation at position 1683 reduced dendritic targeting to 27% of injected cells, indicating that the region between positions 1683 and 2408 contains *cis*-acting element(s) necessary for dendritic targeting. Furthermore, the region upstream of position 1683, including the previously identified localization element (Mori *et al*., 2000), is not sufficient for dendritic targeting in the microinjection assay. Examination of the sequence between positions 1683 and 2408 identified an A2RE-like sequence (GCCAGUGAGCC) at position 2086. Deletion of this sequence reduced dendritic targeting to 25% of injected cells indicating that it is necessary for dendritic targeting. Insertion of the A2RE-like sequence from mouse αCaMKII into GFP RNA increased dendritic targeting to 96% of injected cells, indicating that it is sufficient for dendritic targeting. The A2RE-like sequence in mouse αCaMKII RNA differs from the second A2RE sequence in MBP RNA at one position (G6U). Substitution of C for G at this position (G6C) in MBP A2RE abrogated hnRNP A2 binding and dendritic targeting by the A2 pathway (Munro *et al*., 1999). However, our results indicate that the A2RE sequence in mouse αCaMKII RNA with U at this position binds to hnRNP A2 (Figure 4) and that it is necessary and sufficient for dendritic targeting by the A2 pathway (Figure 2).

TheA2RE sequence identified in mouse αCaMKII RNA is conserved in human, chimp and cow but is precisely deleted in rat αCaMKII RNA (Figure 3). Microinjection of the 3′UTR of rat αCaMKII RNA into neurons resulted in dendritic targeting in 78% of injected cells (Figure 2), indicating that the 3′UTR of rat αCaMKII RNA contains functional dendritic-targeting element(s). Sequence analysis of the 3′UTR of rat αCaMKII RNA identified a different A2RE-like sequence (GGCAAGGAGAG), located ~100 nucleotides upstream of the position corresponding to the A2RE identified in mouse αCaMKII RNA. This A2RE-like sequence in rat αCaMKII RNA is partially deleted in mouse αCaMKII RNA (Figure 3). Deletion of the A2RE-like sequence from the 3′UTR of rat αCaMKII RNA reduced dendritic targeting to 22% of injected cells, indicating that it is necessary for dendritic targeting and that previously identified localization elements in rat αCaMKII RNA (Mori *et al*., 2000; Blichenberg *et al*., 2001) are not required for dendritic targeting in this assay. Insertion of the A2RE-like sequence from rat αCaMKII RNA into GFP RNA increased dendritic targeting to 76% of injected cells, indicating that it is sufficient for dendritic targeting. The A2RE sequence in rat αCaMKII RNA differs from the first A2RE sequence in MBP RNA at three positions (C2G, C10A, and C11G). Substitutions at these positions in MBP A2RE do not prevent binding of MBP A2RE to hnRNP A2 or dendritic targeting by

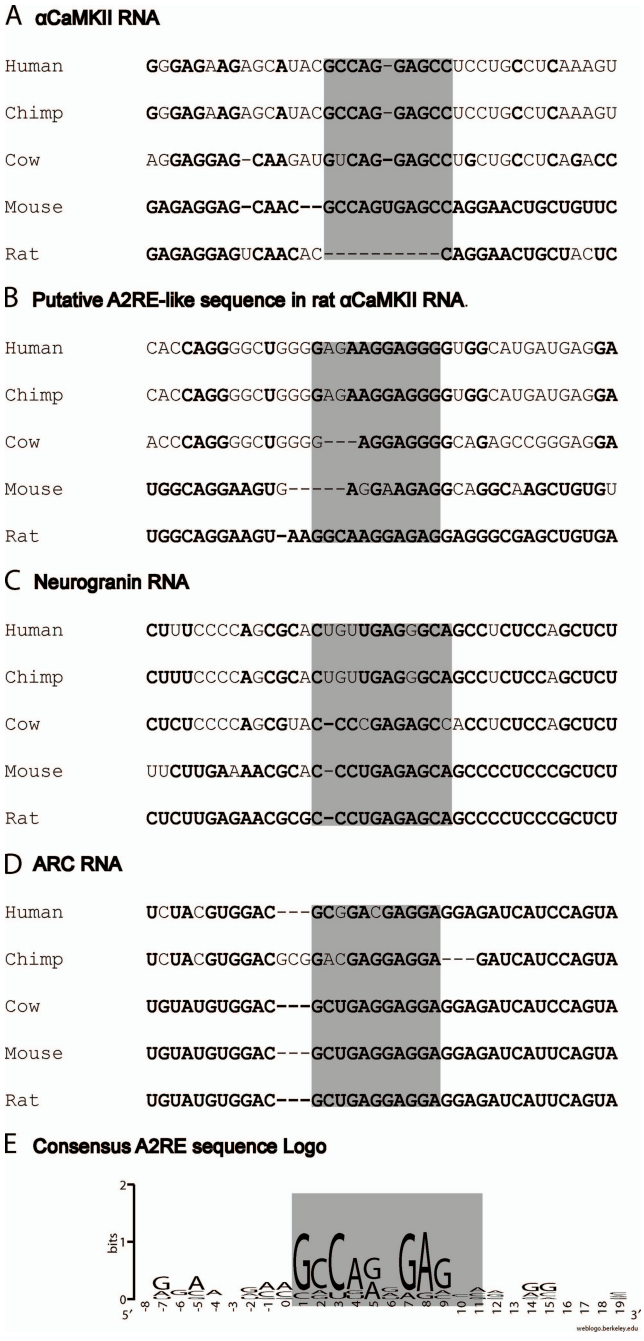

Figure 3. Conservation of A2REs in αCaMKII, NG, and ARC RNAs. A2RE-like sequences with 15 bases of flanking sequence in mouse αCaMKII RNA (A), rat αCaMKII RNA (B), rat NG RNA (C), and rat ARC RNA (D) are compared in human, chimp, cow, mouse, and rat. The A2RE-like sequence is shaded, conserved positions are bold. Deletions are indicated by dashes. A consensus A2RE sequence logo (E) was calculated based on A2RE-like sequences from rat MBP, mouse αCaMKII RNA, rat αCaMKII RNA, rat NG, rat ARC, rat PKMζ RNA, HIV gag, and HIV vpr.

the A2 pathway (Munro *et al*., 1999). The fact that A2RE-like sequences are located at different positions in mouse and rat αCaMKII RNAs indicates that the dendritic targeting function of the A2RE is position independent.

Full-length NG RNA (1-1383) was targeted to dendrites in 70% of injected cells. Truncation at position 1092 reduced dendritic targeting to16% of injected cells, indicating that a *cis*-acting element located downstream of position 1092 is necessary for dendritic targeting. Examination of the sequence downstream of position 1092 identified an A2RE-like sequence (CCCUGAGAGCA) at position 1169 that is similar to the A2RE sequence identified in αCaMKII RNA. Deletion of this sequence reduced dendritic targeting to 22% of injected cells, indicating that it is necessary for dendritic targeting and that the previously identified localization element in NG RNA (Mori *et al*., 2000) is not required for dendritic targeting in this assay. Insertion of the A2RE-like sequence from NG RNA into GFP RNA increased dendritic targeting to 81% of injected cells, indicating that it is sufficient for dendritic targeting. The A2RE-like sequence in NG RNA differs from the second A2RE in MBP RNA at three positions (G1C, A4U, and C11A). Substitutions at these positions in MBP A2RE do not prevent binding to hnRNP A2 or dendritic targeting by the A2 pathway (Munro *et al*., 1999).

Full-length ARC RNA (1-3032) was targeted to dendrites in 71% of injected cells. Truncation at position 1303 did not affect dendritic targeting, indicating that the region downstream of 1303 does not contain elements necessary for dendritic targeting. Truncation at position 1064 reduced dendritic targeting to 35% of injected cells indicating that the region from 1064 to 1303 contains *cis*-acting dendritic-targeting elements(s). Examination of the sequence in this region identified an A2RE-like sequence (GCUGAGGAGGA) at position 1162 that is similar to A2RE sequences identified in αCaMKII and NG RNAs. Deletion of this sequence reduced dendritic targeting to 30% of injected cells, indicating that it is necessary for dendritic targeting and that the previously identified localization element in ARC RNA (Kobayashi *et al*., 2005) is not required for dendritic targeting in this assay. Insertion of the A2RE-like sequence from ARC RNA into GFP RNA increased dendritic targeting to 75% of injected cells, indicating that it is sufficient for dendritic targeting. The A2RE sequence in ARC RNA differs from the first MBP A2RE at four positions (C3U, A4G, C10G, and C11A). Substitutions at these positions in MBP A2RE do not prevent binding to hnRNP A2 or dendritic targeting by the A2 pathway (Munro *et al*., 1999).

Dendritic targeting of PKMζ RNA was not analyzed in this study. However, a previous study using a similar microinjection assay to identify dendritic localization elements in PKMζ RNA delineated a *cis*-acting element in the 3′UTR containing an A2RE-like sequence (GCCAGAGAGGG) that differs from the second A2RE in MBP RNA at two positions (C10G and C11G) (Muslimov *et al*., 2004). Substitutions at these positions in MBP A2RE do not prevent binding to hnRNP A2 or dendritic targeting by the A2 pathway (Munro *et al*., 1999). This suggests that dendritic targeting of PKMζ RNA is mediated by a *cis*-acting A2RE sequence similar to the A2RE sequences identified for αCaMKII, NG, and ARC RNAs.

That αCaMKII, NG, ARC, and PKMζ RNAs all contain similar *cis*-acting A2RE dendritic targeting determinants suggests that these RNAs follow the same pathway. That dendritic targeting determinants identified by the microinjection assay differ from localization elements identified previously in these RNAs by in situ hybridization of heterologous reporter RNAs suggests that the microinjection assay measures a different aspect of dendritic targeting than the in situ hybridization assays used in previous studies.

A2RE-like Sequences in αCaMKII, NG, and ARC RNAs Are Conserved

A2RE sequences in αCaMKII, NG, and ARC RNAs along with 15 bases of 5′-and 3′-flanking sequence were compared

in human, chimp, cow, rat, and mouse (Figure 3). A2RE sequences are more highly conserved than flanking regions, even in ARC RNA where the A2RE sequence is located in the ORF. The one exception is rat αCaMKII RNA where the A2RE sequence identified in mouse αCaMKII RNA is precisely deleted with a compensatory A2RE sequence inserted ~100 base pairs upstream. Conservation of A2RE sequences in different species and the existence of A2RE sequences at different positions in mouse and rat αCaMKII RNA suggest that A2RE-mediated dendritic targeting is a conserved function in these RNAs.

A2RE sequences in MBP, HIV, αCaMKII, NG, ARC, and PKMζ RNAs were used to define a consensus A2RE sequence logo. The sequence logo indicates that positions 1–5 and 7–9 in the A2RE are most highly conserved, whereas positions 6, 10, and 11 are less conserved. Highly conserved positions may reflect base-specific contacts with hnRNP A2. Alternatively, complementary base pairing between the A2RE sequence and other sequences in the RNA may constrain certain positions. In this regard, Muslimov proposed that A2RE-like sequences in MBP, PKMζ, and BC1 RNA are contained within larger "kink-turn" secondary structure motifs (Muslimov *et al*., 2006). If A2RE sequences in αCaMKII, NG, and ARC RNAs are also contained within secondary structure motifs that are necessary for hnRNP A2 binding and dendritic targeting by the A2 pathway, this could constrain certain positions in the A2RE-like sequence.

A2REs in αCaMKII, NG, and ARC RNAs Bind to hnRNP A2 In Vitro

Binding of different A2RE sequences to hnRNP A2 was analyzed by SPR and FCCS (Figure 4). SPR measures changes in refractive index when soluble analyte (A2RE oligonucleotides) binds to immobilized ligand (hnRNP A2). Change in refractive index over time is recorded as a sensorgram, providing a measure of association and dissociation kinetics. Kinetic constants (k_a and k_d) are determined by fitting sensorgram data to a particular biophysical binding model. Affinity constants (K_D) are calculated as the ratio of k_d/k_a. Because hnRNP A2 contains two RNA recognition motifs and because previous studies identified both specific and nonspecific binding sites in hnRNP A2 (Shan *et al*., 2000), SPR data were fitted to a heterogeneous two-site ligand model to determine separate on rates (k_a) off rates (k_d) and affinity constants (K_D) for each binding site. It is possible that the SPR data could be fitted equally well with a different model but the two-site model is consistent with the known structure of hnRNP A2 and with previous reports of specific and nonspecific binding sites in hnRNP A2 (Shan *et al*., 2000). Sensorgrams for A2RE sequences from rat MBP, mouse αCaMKII, rat αCaMKII, rat NG, rat ARC, and rat PKMζ RNAs and for antisense MBP A2RE sequence as a nonspecific binding control are shown in Figure 4, A–G. Maximum amplitudes are different for different A2RE sequences because the association phase was terminated before equilibrium was reached.

Kinetic constants and affinity constants for binding of each A2RE sequence to sites 1 and 2 in hnRNP A2 are summarized in Figure 4M. Most A2RE sequences bind more rapidly to site 2 (k_{a2} = 50–500 × 10^4 M^{-1} s^{-1}) than to site 1 (k_{a1} = 1–10 × 10^4 M^{-1} s^{-1}). ARC and NG A2REs have slower on rates for both sites, perhaps indicating that these sequences form secondary structures that interfere with binding to hnRNP A2. Off rates for most A2RE sequences are comparable at both sites ($k_{d1,2}$ = 10–100 × 10^{-4} s^{-1}) except for ARC and PKMζ A2RE, which have slower off rates at site 1, perhaps due to stronger sequence specific binding at this site. A nonspecific control sequence shows very slow binding to hnRNP A2. These results indicate that each hnRNP A2 molecule contains two separate A2RE RNA binding sites, one site with a slower on rate and one site with a faster on rate. In addition, hnRNP A2 exhibits nonspecific binding to RNA.

Binding affinities were also measured by FCCS, which measures fluorescence fluctuations when differentially labeled fluorescent molecules (hnRNP A2 and A2RE oligoribonucleotides) diffuse together through the FCS observation volume. The amplitude of the autocorrelation function in each channel provides a measure of total concentration for each fluorescent species. The amplitude of the cross correlation function provides a measure of concentration of the bound complex, which can be used to calculate the K_D. FCCS binding isotherms for binding of hnRNP A2 to A2RE sequences from rat MBP, mouse αCaMKII, rat NG, rat ARC RNAs, and antisense are shown in Figure 4, H–L. FCCS does not resolve separate K_D values for each binding site in hnRNP A2. Overall K_D values measured by FCCS are comparable (K_D = 5–20 nM) for different A2RE sequences and intermediate between individual K_D values for each binding site in hnRNP A2 determined by SPR. The K_D for binding to antisense A2RE could not be determined by FCCS because concentrations of fluorescent molecules >100 nM cannot be measured accurately by FCS.

High-affinity sequence-specific binding of A2RE sequences to hnRNP A2 may provide the basis for selectivity in distinguishing A2RE from non-A2RE RNAs in the A2 pathway. A putative A2RE-like sequence from BC1 RNA (Muslimov *et al*., 2006) did not bind with high-affinity to hnRNP A2 (data not shown), suggesting that this sequence does not mediate dendritic targeting of BC1 RNA by the A2 pathway. Because hnRNP A2 binds with high-affinity to synthetic A2RE oligonucleotides, which presumably have little secondary structure, interaction with hnRNP A2 may not require extensive secondary structure.

Antibody to hnRNP A2 Inhibits Dendritic Targeting of αCaMKII, NG, and ARC RNAs

Previous studies in oligodendrocytes (Munro *et al*., 1999) and neurons (Shan *et al*., 2003) showed that reducing hnRNP A2 expression by using antisense oligonucleotides inhibited dendritic targeting of A2RE RNA. However, these experiments do not prove that hnRNP A2 is directly required as a *trans*-acting factor for dendritic targeting. Because hnRNP A2 is involved in many cellular processes (telomere metabolism, splicing, and nuclear export) that are unrelated to RNA trafficking, prolonged reduction of hnRNP A2 expression by antisense oligonucleotide may secondarily affect expression of off-target factors required for dendritic targeting or perturb cell physiology in other ways. To inhibit hnRNP A2 function directly, antibody to hnRNP A2 (0.5 mg/ml) was coinjected with RNA (Figure 5). Coinjection of antibody to hnRNP A2 reduced dendritic targeting of αCaMKII, NG, and ARC RNAs, whereas coinjection of antibody to GFP did not, indicating that hnRNP A2 is directly involved as a *trans*-acting factor for dendritic targeting of A2RE RNAs. The injected antibody recognizes a sequence of 18 residues at the C terminus of hnRNP A2 (Nichols *et al*., 2000), which is a region of the molecule implicated in binding to transportin 1 during nuclear import and to tumor overexpressed gene (TOG) protein during granule assembly (Carson *et al*., 2006). Antibody binding to this region may interfere with hnRNP A2 binding to transportin and/or TOG protein, thereby disrupting nuclear transport and/or granule assembly in the A2 RNA trafficking pathway.

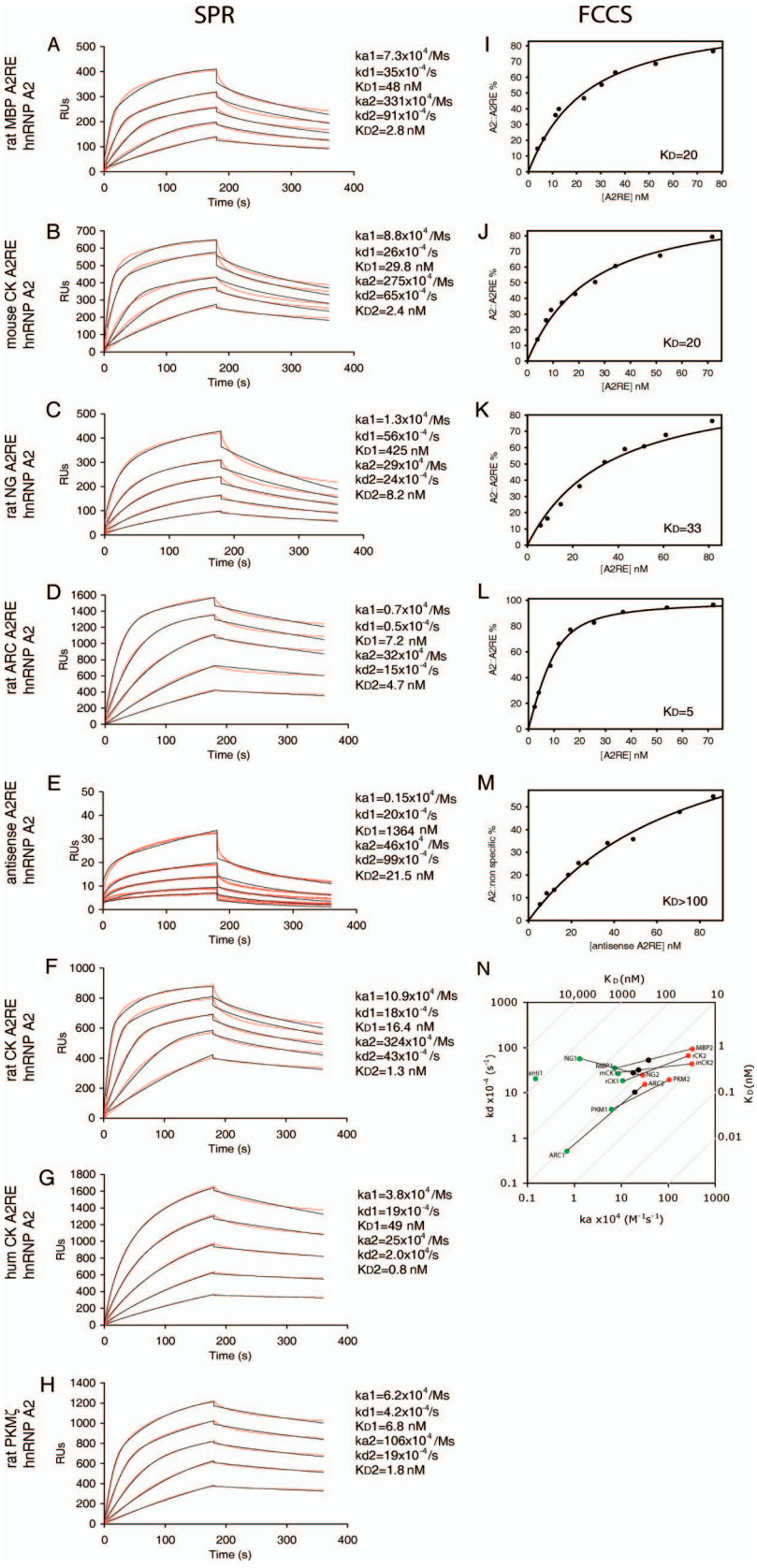

Figure 4. Binding of A2REs to hnRNP A2. SPR measurements were performed with ligand consisting of recombinant hnRNP A2 covalently coupled to a CM5 chip and analyte consisting of biotinylated oligoribonucleotides corresponding to the A2REs from the following RNAs: rat MBP RNA (A), mouse αCaMKII RNA (B), rat NG RNA (C), rat ARC RNA (D), rat MBP A2RE antisense (E), rat αCaMKII RNA (F), and rat PKMζ RNA (G), injected at 12.5, 25, 50, 100, and 200 nM. Sensorgram data (red) was fitted to a heterogenous ligand model (black). Binding isotherms (H–L) determined by FCCS are shown on the right. Binding constants (k_a, k_d, and K_D) for sites 1 (green dots) and 2 (red dots) measured by SPR, and overall K_D values measured by FCCS (black dots) are compared in M.

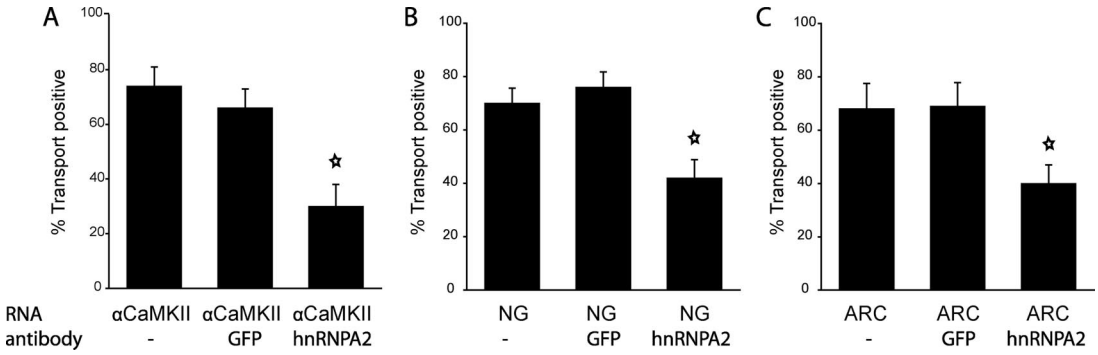

Figure 5. Antibody to hnRNP A2 inhibits dendritic targeting of αCaMKII RNA. Antibody to either hnRNP A2 or GFP was coinjected (0.5 mg/ml in the needle) into hippocampal neurons along with fluorescent αCaMKII, NG, or ARC RNA. Transport positive cells were determined as described in *Material and Methods*. At least 50 cells were analyzed for each combination of antibody and RNA. The stars indicate dendritic targeting measurements that are different from untreated cells with >99.6% confidence by Fisher's exact test (Fisher, 1922).

αCaMKII, NG, and ARC RNA Granules Contain hnRNP A2

Colocalization of hnRNP A2 with exogenous αCaMKII, NG, and ARC RNAs was analyzed in hippocampal neurons injected with fluorescent RNAs and differentially stained with antibody to hnRNP A2 (Figure 6). Colocalization of hnRNP A2 with endogenous αCaMKII, NG, and ARC RNAs in hippocampal neurons was analyzed by FISH for endogenous αCaMKII, NG, and ARC RNA combined with differential immunostaining for hnRNP A2 (Figure 7). Colocalization was quantified using two methods. The first method, single granule ratiometric analysis (Barbarese *et al*., 1995), provides a measure of the relative amounts RNA and hnRNP A2 in individually selected well-resolved granules. Greater than 80% of granules containing exogenous or endogenous αCaMKII, NG, or ARC RNA granules also contained hnRNP A2. Granules containing hnRNP A2 but deficient in exogenous RNA may have been assembled and localized before injection of fluorescent RNA. The second method, image cross-correlation analysis, provides a measure of overall cross correlation between fluorescent RNA and hnRNP A2 in dendrites. Compared with single granule ratiometric analysis, image correlation analysis is based on a larger statistical sample of pixels consisting of extended regions of dendrites; therefore, it can measure overall colocalization more accurately. Image correlation is also more objective because it does not involve manual selection of individual granules. The amplitude of the image correlation function provides a measure of Pearson's r, which was >0.3 for colocalization of exogenous and endogenous αCaMKII, NG, or ARC RNAs with hnRNP A2. Decay of the image cross-correlation function over distance provides a measure of the size distribution of cellular structures responsible for colocalization. Both exogenous and endogenous αCaMKII, NG and ARC RNA showed a predominant component that decayed over a distance of <1 μm, presumably corresponding to RNA granules. Colocalization of exogenous and endogenous αCaMKII, NG, and ARC RNAs with hnRNP A2 in structures the size of RNA granules is consistent with dendritic targeting by the A2 trafficking pathway.

Electroconvulsive Shock Causes Accumulation of hnRNP A2 in Dendrites

ECS results in induction and dendritic targeting of ARC RNA in the hippocampus (Lyford *et al*., 1995). To determine whether ECS results in increased numbers of hnRNP A2-containing granules and/or increased amounts of hnRNP A2 per granule, rats were subjected to ECS and the hippocampus was sectioned and stained with antibody to hnRNP A2 (Figure 8). In control rats, hnRNP A2 granules were detected in the dendritic layer of the CA1 region of the hippocampus, consistent with dendritic targeting of constitutively expressed A2RE RNAs such as αCaMKII and NG RNA by the A2 pathway. In ECS-treated rats both the number of hnRNP A2 granules and the amount of hnRNP A2 per granule were increased in the dendritic layer of the CA1 region, consistent with induction and dendritic targeting of ARC RNA by the A2 pathway after ECS. The average number of hnRNP A2 granules per 100 μm^2 was 24 ± 4 for control and 33 ± 3 for ECS-treated animals, indicating that increased numbers of granules are assembled after ECS. The average intensity of hnRNP A2 per granule was 109 ± 16 for control and 154 ± 7 for ECS-treated animals, indicating that increased amounts of hnRNP A2 are assembled into each granule after ECS. These results are consistent with dendritic targeting of ARC RNA by the A2 pathway.

αCaMKII, NG, and ARC RNAs Are Coassembled into the Same Granules

Coassembly of exogenous αCaMKII, NG, and ARC RNAs into the same granules was analyzed by coinjecting pairwise combinations of differentially labeled RNAs into hippocampal neurons (Figure 9). Coassembly of endogenous αCaMKII, NG, and ARC RNAs into granules was analyzed by coFISH for pairwise combinations of RNAs in hippocampal neurons (Figure 10). Colocalization was quantified by single granule ratiometric analysis and image-cross correlation analysis. For each pairwise combination of exogenous αCaMKII, NG, and ARC RNAs, >70% of granules contained both RNAs, with >0.6 overall cross-correlation, indicating that these injected RNAs are coassembled into the same granules. In cells coinjected with NG RNA and GFP RNA, dendritically targeted granules contained predominantly NG RNA with little GFP RNA, indicating that GFP RNA is not targeted to dendrites and that it is not efficiently assembled into granules containing NG RNA. Despite the low amount of GFP RNA associated with most NG RNA granules, overall cross-correlation was ~0.35, which presumably reflects misassembly of a small number of GFP RNA molecules into NG RNA granules. For each pairwise combination of endogenous αCaMKII, NG, and ARC RNAs, >50% of granules contain both RNAs with >0.3 overall cross-correlation, indicating that these endogenous RNAs are coassembled into the same granules. αCaMKII and β-actin RNA, a non-A2RE RNA

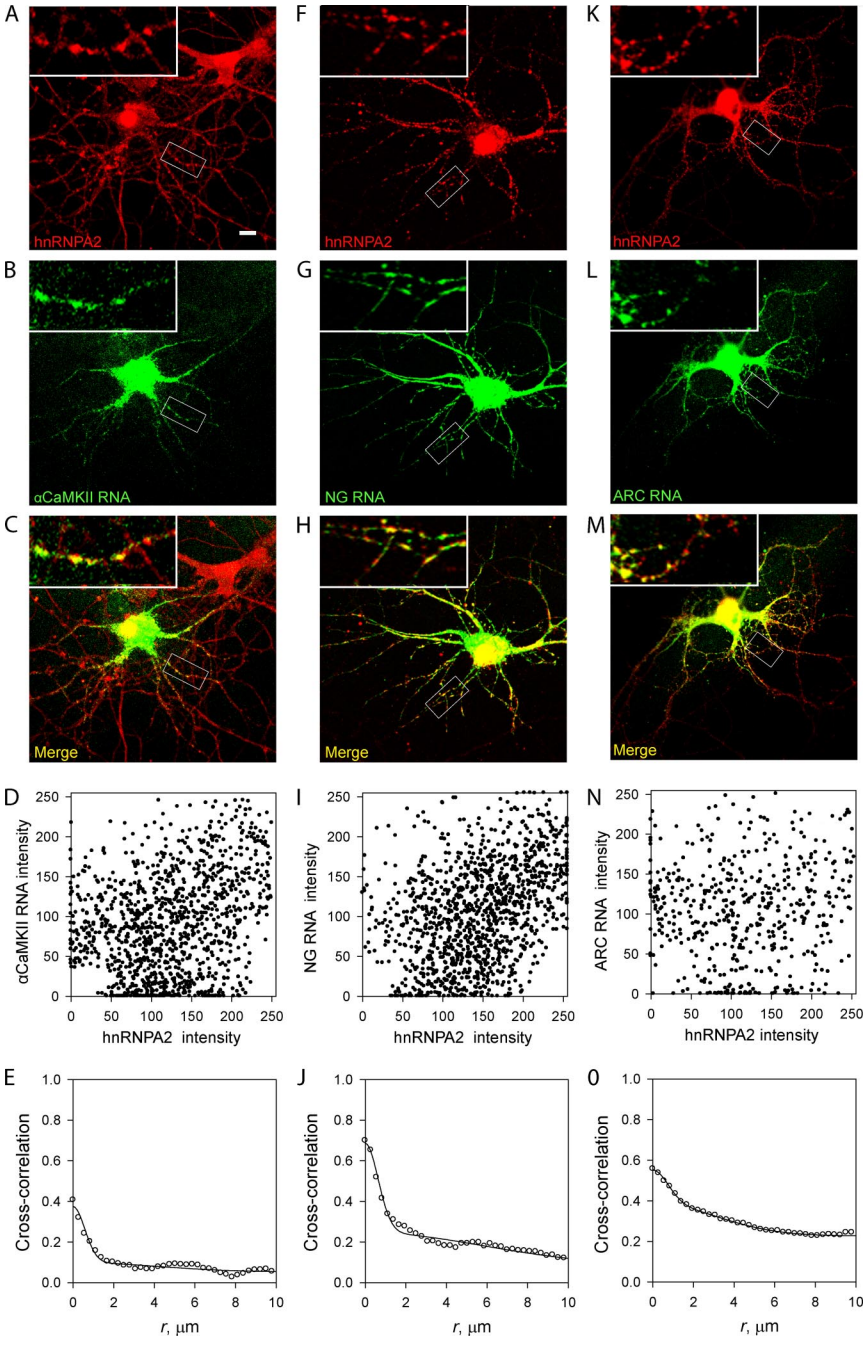

Figure 6. Colocalization of exogenous αCaMKII, NG, and ARC RNAs with hnRNP A2. Fluorescent αCaMKII, NG, and ARC RNAs (green) were microinjected into hippocampal neurons. After allowing time for transport (30–45 min), cells were fixed and differentially stained with antibody to hnRNP A2 (red). Bar, 10 μm. Insets at higher magnification reveal individual granules. Colocalization was quantified by single granule ratiometric analysis and image-cross correlation analysis. A, F, and K show hnRNP A2 distribution in representative cells. B,G, and L show distributions of αCaMKII, NG, and ARC RNA, respectively, in the same cells. C, H, and M show merged images of hnRNP A2 and RNA in each cell. D, I, and N show ratiometric analysis of colocalization of hnRNP A2 and αCaMKII, NG and ARC RNAs, respectively. E, J, and O show image cross-correlation analysis of hnRNP A2 and αCaMKII, NG, and ARC RNAs, respectively.

(Tiruchinapalli *et al.*, 2003), were predominantly segregated into separate granules, with ~0.2 overall correlation due to occasional misassembly of actin RNA into αCaMKII RNA granules and vice versa.

Variance in proportions of different A2RE RNAs among individual granules was greater for endogenous than for exogenous A2RE RNAs. According to the central limit theorem, variance in proportions of objects among samples (proportions of RNA molecules among granules) is inversely proportional to sample size (number of fluorescent RNA molecules per granule). Increased variance in endogenous RNAs compared with exogenous RNAs may mean that the number of endogenous RNA molecules per granule is smaller than the number of exogenous RNA molecules per granule or that different endogenous RNAs are expressed at different levels, whereas exogenous RNAs are injected in equivalent amounts. It is not known whether exogenous αCaMKII, NG, and ARC RNA molecules assemble onto pre-existing granules or coassemble into new granules.

If coinjected A2RE RNAs assemble onto pre-existing granules that are already localized in dendrites, colocalized RNAs may be relatively immobile. However, if coinjected RNAs coassemble into new granules that are targeted to dendrites, colocalized RNAs may be cotransported to dendrites in the same granules. To visualize cotransport of different A2RE RNAs in the same granule, differentially labeled αCaMKII and ARC RNAs were coinjected into hippocampal neurons and analyzed by dual-channel time-lapse imaging (Supplemental Movie S1). The movie shows three granules in a dendrite of a cell coinjected with αCaMKII

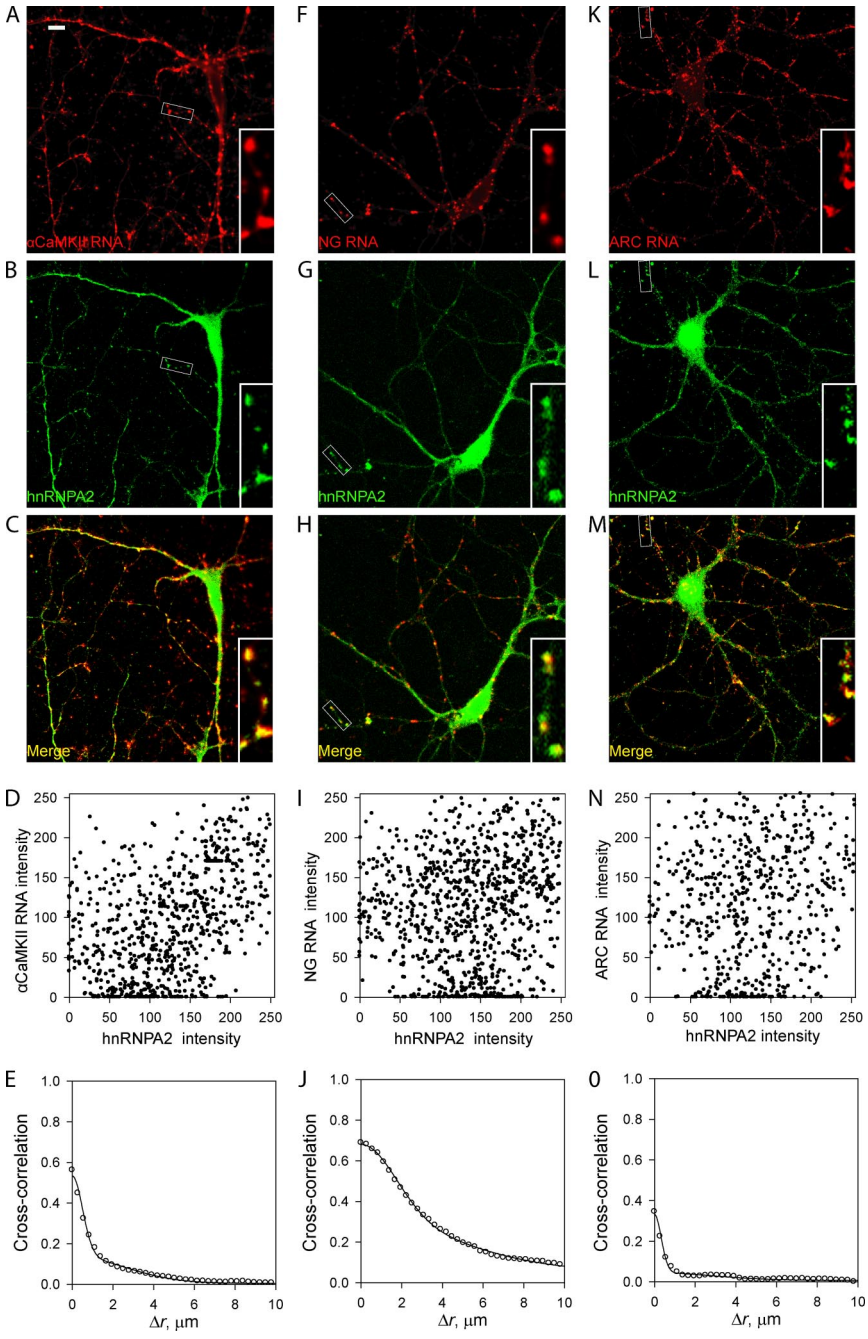

Figure 7. Colocalization of endogenous αCaMKII, NG, and ARC RNAs with hnRNP A2. Endogenous αCaMKII, NG, and ARC RNAs in hippocampal neurons in culture were detected by FISH (green), and hnRNP A2 was detected by immunofluorescence. Bar, 10 μm. Insets at higher magnification reveal individual granules. Colocalization was quantified by single granule ratiometric analysis and image cross-correlation analysis. A, F, and K show distributions of αCaMKII, NG, and ARC RNAs, respectively, in representative cells. B, G, and L show distributions of hnRNP A2 in the same cells. C, H, and M show merged images of hnRNP A2 and RNA in each cell. D, I, and N show ratiometric analysis of colocalization of hnRNP A2 and αCaMKII, NG, and ARC RNAs, respectively. E, J, and O show image cross-correlation analysis of hnRNP A2 and αCaMKII, NG, and ARC RNAs, respectively.

(red) and ARC (green) RNAs. All three granules contain both labeled RNAs. Two of the granules are immobile, but one granule moves bidirectionally along the dendrite. This indicates that two different A2RE RNAs coassembled into the same granule are cotransported in dendrites.

Excess ARC RNA Inhibits Dendritic Targeting of αCaMKII and NG RNAs

Because αCaMKII, NG, and ARC RNAs are coassembled into the same granules and targeted to dendrites by the same pathway, excess amounts of one A2RE RNA may compete with other A2RE RNAs for assembly into granules and dendritic targeting. Injection of excess unlabeled ARC RNA inhibited dendritic targeting of labeled αCaMKII or NG RNA, whereas ARC RNA lacking the A2RE-like sequence did not (Figure 11). This indicates that αCaMKII and NG RNAs are dendritically targeted by the same pathway as ARC RNA, that the pathway is saturable, and that excess ARC RNA competes for some rate-limiting component of the pathway, thereby reducing dendritic targeting of αCaMKII and NG RNAs.

DISCUSSION

αCaMKII, NG, and ARC RNAs contain similar *cis*-acting A2RE sequences that bind to the same *trans*-acting factor, hnRNP A2, to mediate dendritic targeting by the A2 pathway. PKMζ RNA also contains an A2RE-like dendritic-tar-

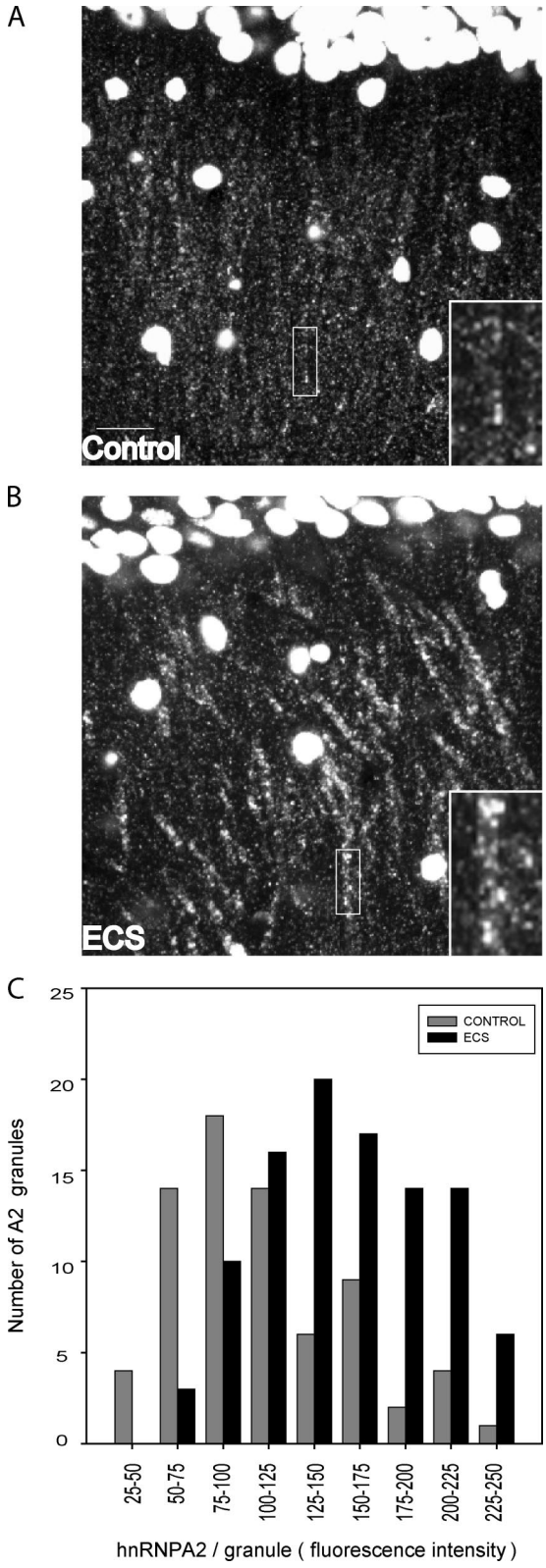

Figure 8. Immunostaining of hnRNP A2 in hippocampus of ECS-treated rats. Brains from three control rats (A) and three rats treated with ECS (B) were sectioned and stained with antibody to hnRNP A2. Representative images of the CA1 region from control and ECS-treated animals are shown with cell nuclei at the top and dendritic layer at the bottom. Bar, 10 μm. Insets at higher magnification reveal individual granules. Individual granules were selected in three different regions of interest (100 μm^2) from images of control and ECS-treated animals and the total number of granules and fluorescence intensity (amount of hnRNP A2) per granule were measured. C shows the overall frequency distribution for number of granules and hnRNP A2 per granule.

geting element (Muslimov *et al*., 2006) that binds to hnRNP A2, suggesting that it follows the same A2 pathway. Thus, the A2 pathway may be a general pathway for multiplexed dendritic targeting of several different A2RE RNAs in hippocampal neurons.

The A2RE dendritic targeting sequences in αCaMKII, NG, and ARC RNAs identified by the microinjection assay are different from previously reported localization elements in these RNAs. One reason may be that previous studies used in situ hybridization to measure steady-state distribution of heterologous RNAs in dendrites, which can be affected by multiple different nuclear and cytoplasmic processes, whereas the microinjection assay specifically measures dendritic targeting while minimizing confounding effects of other processes. This raises two related questions: what specific step(s) in the RNA trafficking pathway is being measured in the microinjection assay and what is the physiological significance of dendritic-targeting elements identified by microinjection compared with localization elements identified by in situ hybridization.

The microinjection assay measures translocation of RNA from perikaryon to dendrites. This could reflect either biased transport of A2RE RNA granules from perikaryon to dendrites or unbiased movement of A2RE RNA granules in dendrites coupled with local immobilization at specific dendritic sites. Because movement of A2RE RNA granules along dendritic microtubules is bidirectional, distinguishing between these two possibilities will require systematic tracking of many individual granules over extended time intervals, which is beyond the scope of this study.

Microinjected RNAs are not translated efficiently because they are not capped or polyadenylated, and they contain fluorophore-conjugated ribonucleotides. In this sense, the injected RNAs represent "artificial" substrates, whose behavior may differ from endogenous RNAs. Despite that they are not capped or polyadenylated the injected fluorescent RNAs are not rapidly degraded in the cell because fluorescence does not accumulate in the nucleus. Furthermore, because translation of RNA is often associated with immobilization, reduced translational efficiency of injected RNAs may allow for more efficient translocation to dendrites by preventing immobilization in the perikaryon. Thus, the artificial properties of the injected RNA may facilitate identification of dendritic targeting elements by facilitating translocation and minimizing confounding effects of translation and RNA degradation. Because the microinjection assay is designed to analyze one specific step (dendritic targeting) in the trafficking pathway, *cis*-acting elements identified using the microinjection assay likely affect the subcellular distribution of endogenous RNAs but may not account for all aspects of RNA physiology.

The physiological significance of dendritic-targeting elements identified by microinjection is also related to the temporal resolution of the microinjection assay, which measures translocation of A2RE RNAs from perikaryon to dendrites during a relatively short time interval (~30 min) after injection. This is comparable with the time course of changes in synaptic sensitivity that occur during learning and memory. By contrast, in situ hybridization studies measure steady state levels of RNA in dendrites reflecting long-term

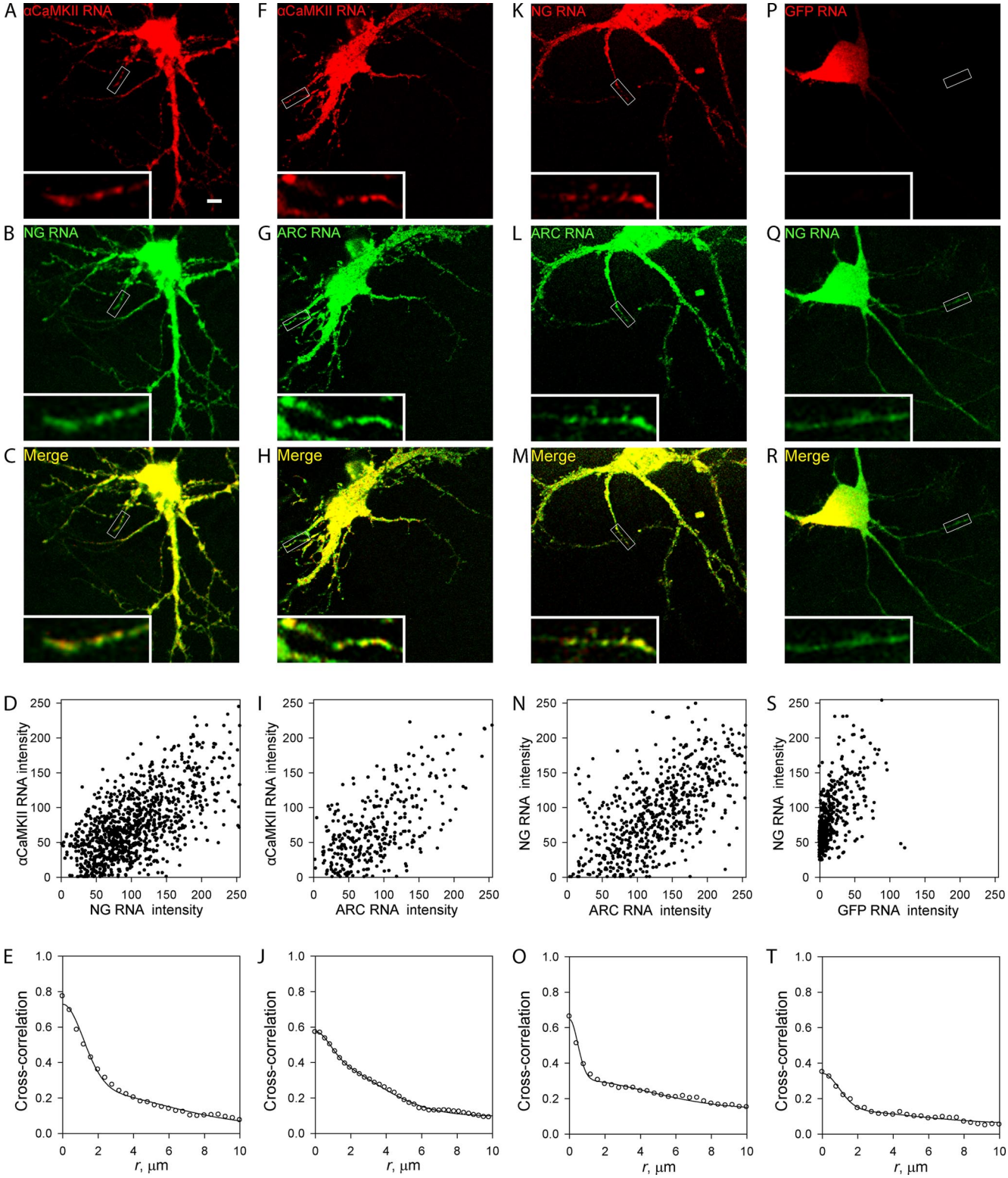

Figure 9. Colocalization of exogenous αCaMKII, NG, and ARC RNAs in granules. Exogenous αCaMKII, NG, and ARC RNAs were differentially labeled and coinjected in pairwise combinations into hippocampal neurons. Coassembly of NG RNA and GFP RNA was also analyzed. Bar, 10 μm. Insets at higher magnification reveal individual granules. Colocalization was quantified by single granule ratiometric analysis and image cross-correlation analysis. A, F, K, and L show distributions of αCaMKII, αCaMKII, NG, and GFP RNAs, respectively, in representative cells. B, G, L, and Q show distributions of NG, ARC, ARC, and NG RNAs in the same cells. C, H, M, and R show merged images of the two RNAs in each cell. D, I, N, and S show single granule ratiometric analysis of colocalization of each pair of RNAs. E, J, O, and T show image cross-correlation analysis of each pair of RNAs.

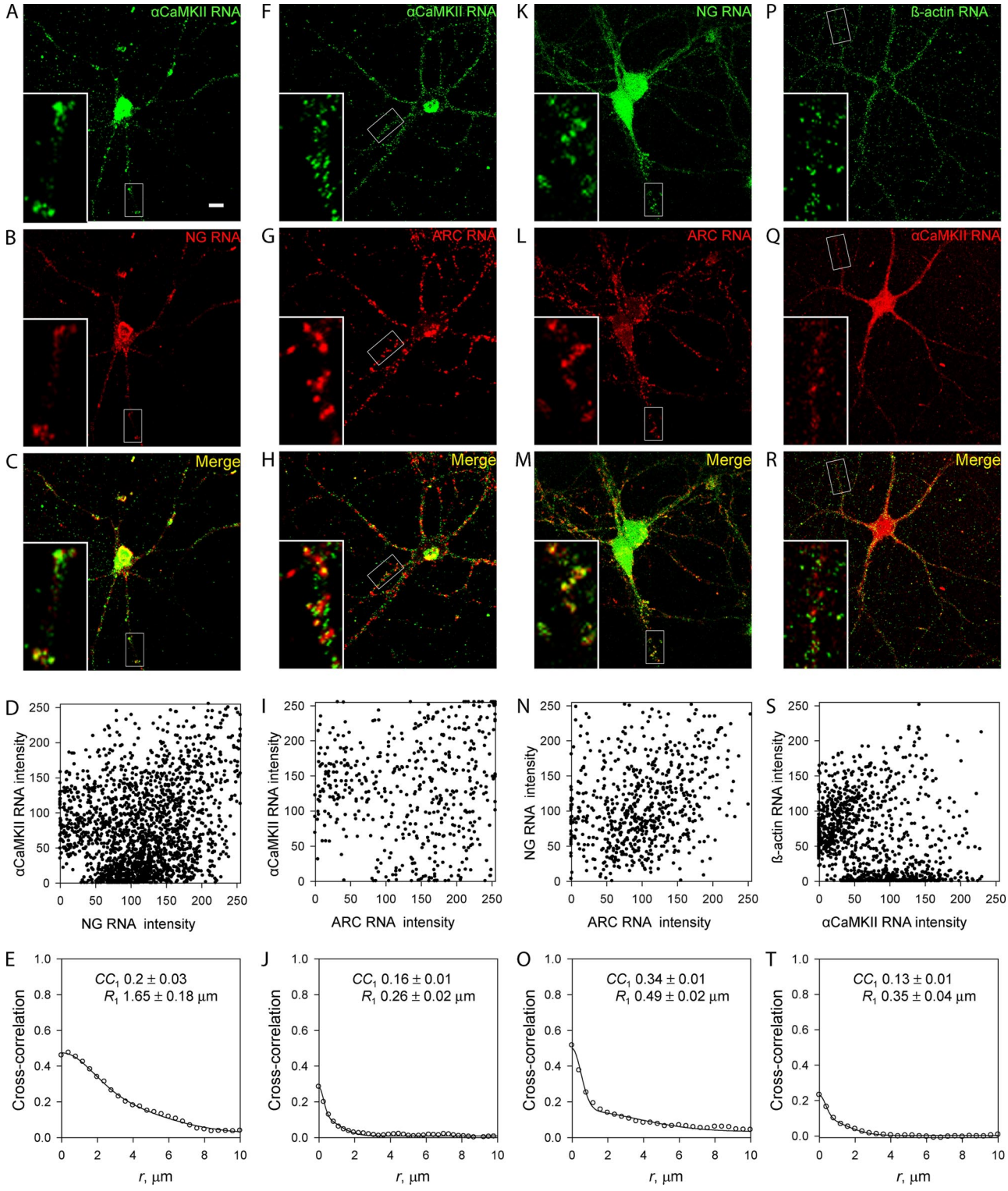

Figure 10. Colocalization of endogenous αCaMKII, NG, and ARC RNAs in granules. Endogenous αCaMKII, NG, ARC, and β-actin RNAs in hippocampal neurons were detected in pairwise combinations by differential fluorescent in situ hybridization. Bar, 10 μm. Insets at higher magnification reveal individual granules. Colocalization was quantified by single granule ratiometric analysis and image cross-correlation analysis. A, F, K, and L show distributions of αCaMKII, αCaMKII, NG, and β-actin RNAs, respectively, in representative cells. B, G, L, and Q show distributions of NG, ARC, ARC, and αCaMKII RNAs in the same cells. C, H, M, and R show merged images of the two RNAs in each cell. D, I, N, and S show single granule ratiometric analysis of colocalization of each pair of RNAs. Panels E, J, O, and T show image cross-correlation analysis of each pair of RNAs.

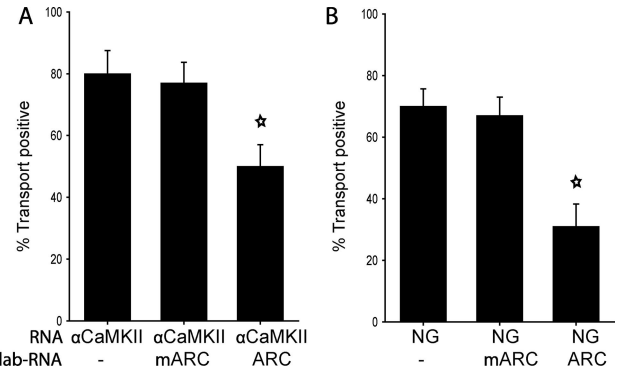

Figure 11. Inhibition of dendritic targeting by excess ARC RNA. Ten-fold excess of unlabeled ARC RNA (ARC) or ARC with the A2RE RNA deleted (mARC) was coinjected into hippocampal neurons along with fluorescent αCaMKII or NG RNA. The percentage of cells with dendritic targeting was determined. The stars indicate dendritic targeting measurements that are different from untreated cells with >99.6% confidence by Fisher's exact test (Fisher, 1922).

stability of RNA in dendrites. αCaMKII, NG, ARC, and PKMζ RNAs are required for rapid changes in synaptic sensitivity during learning and memory. Each of these RNAs contain similar A2RE dendritic targeting sequences, identified by the microinjection assay, but they also contain different *cis*-acting elements, identified by in situ hybridization studies, that mediate steady-state levels in dendrites. This suggests that rapid changes in synaptic sensitivity associated with learning and memory involve multiplexed dendritic targeting of an ensemble of A2RE RNAs by the A2 pathway, whereas steady-state levels of individual A2RE RNAs in dendrites are differentially regulated.

There are three requirements for multiplexed dendritic targeting of A2RE RNAs: a multiplexer (mux) to combine multiple messages (RNA molecules) into a single composite signal (RNA granule), a carrier (microtubules) to transmit the multiplexed signal, and a demultiplexer (demux) (translation machinery) to decompose the multiplexed signal into individual messages. Multiplexing bandwidth is determined by the number of RNA molecules per granule.

The mux in the A2 pathway performs three functions: selection, linkage, and suppression. Selection distinguishes A2RE RNAs from non-A2RE RNAs, which is accomplished by sequence specific binding of hnRNP A2 to A2RE sequences in different RNAs. Initial binding of hnRNP A2 to endogenous A2RE RNAs probably occurs in the nucleus where the concentration of hnRNP A2 is very high. This marks the RNA for subsequent targeting by the A2 pathway when it reaches the cytoplasm. Binding of hnRNP A2 to exogenous RNAs microinjected into the cytoplasm occurs because the concentration of hnRNP A2 in the cytoplasm still exceeds the K_D for binding to A2RE sequences (Kosturko *et al*., 2006). Linkage combines multiple A2RE RNAs into composite granules. This may be accomplished by TOG protein, a granule component that contains multiple binding sites for hnRNP A2 and may function as a multivalent scaffold for coassembly of multiple A2RE RNAs bound to hnRNP A2 molecules into granules (Kosturko *et al*., 2005; Carson *et al*., 2006). In postmitotic cells such as neurons, TOG is restricted to the cytoplasm so linkage presumably occurs in the cytoplasm rather than in the nucleus. Suppression prevents translation of RNAs in granules during transmission from nucleus to synapse. This may be accomplished by hnRNP E1, which is a granule component that binds to hnRNP A2 and inhibits translation of A2RE RNAs (Kosturko *et al*., 2006).

The demux in the A2 pathway involves translation of individual A2RE RNAs into protein, mediated by protein synthetic machinery associated with each granule. If a single granule is captured at an individual synapse demulitplexing results in local translation of multiple different A2RE RNAs at that synapse. In this way, the ensemble of multiplexed A2RE RNAs in the granule determines the pattern of gene expression at the synapse. Because the A2RE is sufficient for dendritic targeting, virtually any RNA can be targeted to dendrites by inserting an A2RE into its sequence. If heterologous RNA is targeted to dendrites in this way, the encoded protein will be expressed locally at synapses, thereby altering synaptic properties. In this way, A2RE-mediated dendritic targeting of heterologous RNA by the A2 pathway could be used to transform synapses.

In addition to facilitating transmission of genetic information from nucleus to synapse, multiplexing also provides a mechanism for spatial and temporal coordination of gene expression at the synapse. Because αCaMKII and NG have opposing effects on synaptic sensitivity, multiplexed dendritic targeting of these RNAs may play a role in tuning synaptic sensitivity. Granules that contain more αCaMKII RNA may cause increased local synthesis of αCaMKII resulting in increased synaptic sensitivity, whereas granules that contain more NG RNA may cause increased local synthesis of NG, resulting in decreased synaptic sensitivity. Because ARC and PKMζ have opposing effects on synaptic scaling, multiplexed dendritic targeting of these RNAs may be important for scaling synaptic strength during long-term potentiation. Granules with more ARC RNA will result in increased local synthesis of ARC, reducing numbers of α-amino-3-hydroxy-5-methyl-4-isoxazolepropionic acid (AMPA) receptors at the synapse, whereas granules with more PKMζ RNA will result in increased local synthesis of PKMζ increasing numbers of AMPA receptors at the synapse. In this way, random variation in granule composition can contribute to stochasticity in postsynaptic responsiveness.

Because the multiplexing mechanism is saturable, competition among different A2RE RNAs can affect the composition of individual granules. RNAs such as αCaMKII and PKMζ with A2REs that bind to hnRNP A2 with fast on rates may be assembled preferentially into RNA granules. Induction of ARC and PKMζ RNAs after synaptic activity may reduce dendritic targeting of NG and αCaMKII RNAs by competing for the A2 pathway. It may be possible to use competition among A2RE RNAs to systematically identify RNAs targeted by the A2 pathway. RNAs whose dendritic targeting is inhibited by excess A2RE RNA are likely to be targeted to dendrites by the A2 pathway. The rate-limiting component in the A2 pathway may not be hnRNP A2 itself, which is present in very high concentrations in most cells (Kosturko *et al*., 2006). A more likely possibility is TOG protein, which is present in lower concentrations in the cytoplasm where it binds to hnRNP A2 and is a component of RNA granules (Kosturko *et al*., 2005).

In summary, multiplexed dendritic targeting of multiple A2RE RNAs by the A2 pathway provides a mechanism for facilitating transmission of genetic information from nucleus to synapse, suppressing translation of dendritic RNAs during transport, coordinating expression of functionally related proteins at synapses, introducing variation in gene expression among synapses, and transforming synapses.

ACKNOWLEDGMENTS

Plasmid containing mouse αCaMKII cDNA was obtained from Dr. M. Mayford, rat αCaMKII cDNA was obtained from Dr. S. Kindler, NG cDNA was obtained from Dr. J. B. Watson, and ARC cDNA was obtained from Dr. P. Worley. Antibody to hnRNP A2 was obtained from Dr. W. Rigby. ECS experiments were performed with the assistance of Dr. X. Ming (University of Connecticut Health Center, Farmington CT). This work was supported by National Institutes of Health grants NS-15190, RR-13186, RR-022232, and RR-022624 (to J.H.C.).

REFERENCES

Ainger, K., Avossa, D., Morgan, F., Hill, S. J., Barry, C., Barbarese, E., and Carson, J. H. (1993). Transport and localization of exogenous myelin basic protein mRNA microinjected into oligodendrocytes. J. Cell Biol. *123*, 431–441.

Ainger, K., Avossa, D., Diana, A. S., Barry, C., Barbarese, E., and Carson, J. H. (1997). Transport and localization elements in myelin basic protein mRNA. J. Cell Biol. *138*, 1077–1087.

Barbarese, E., Koppel, D. E., Deutscher, M. P., Smith, C. L., Ainger, K., Morgan, F., and Carson, J. H. (1995). Protein translation components are colocalized in granules in oligodendrocytes. J. Cell Sci. *108*, 2781–2790.

Benson, D. L., Gall, C. M., and Isackson, P. J. (1992). Dendritic localization of type II calcium calmodulin-dependent protein kinase mRNA in normal and reinnervated rat hippocampus. Neuroscience *46*, 851–857.

Birgbauer, E., Rao, T. S., and Webb, M. (2004). Lysolecithin induces demyelination in vitro in a cerebellar slice culture system. J. Neurosci. Res. *78*, 157–166.

Blichenberg, A., Rehbein, M., Muller, R., Garner, C. C., Richter, D., and Kindler, S. (2001). Identification of a cis-acting dendritic targeting element in the mRNA encoding the alpha subunit of Ca2+/calmodulin-dependent protein kinase II. Eur. J. Neurosci. *13*, 1881–1888.

Carson, J. H., Worboys, K., Ainger, K., and Barbarese, E. (1997). Translocation of myelin basic protein mRNA in oligodendrocytes requires microtubules and kinesin. Cell Motil. Cytoskeleton *38*, 318–328.

Carson, J. H., Blondin, N., and Korza, G. (2006). Rules of engagement promote polarity in RNA trafficking. BMC Neurosci. *7* (suppl 1), S3.

Czaplinski, K., and Singer, R. H. (2006). Pathways for mRNA localization in the cytoplasm. Trends Biochem. Sci. *31*, 687–693.

Farina, K. L., and Singer, R. H. (2002). The nuclear connection in RNA transport and localization. Trends Cell Biol. *12*, 466–472.

Farkas, D. L., Wei, M. D., Febbroriello, P., Carson, J. H., and Loew, L. M. (1989). Simultaneous imaging of cell and mitochondrial membrane potentials. Biophys. J. *56*, 1053–1069.

Fisher, R. A. (1922). On the interpretation of χ^2 from contingency tables, and the calculation of P. J. R. Stat. Soc. *85*, 87–94.

Giorgi, C., and Moore, M. J. (2007). The nuclear nurture and cytoplasmic nature of localized mRNPs. Semin. Cell Dev. Biol. *18*, 186–193.

Goslin, K., and Banker, G. (1989). Experimental observations on the development of polarity by hippocampal neurons in culture. J. Cell Biol. *108*, 1507–1516.

Guadano-Ferraz, A., Vinuela, A., Oeding, G., Bernal, J., and Rausell, E. (2005). RC3/neurogranin is expressed in pyramidal neurons of motor and somatosensory cortex in normal and denervated monkey. J. Comp. Neurol. *493*, 554–570.

Ephrussi, O., and Hachet, A. (2004). Splicing of oskar RNA in the nucleus is coupled to its cytoplasmic localization. Nature *428*, 959–963.

Hoek, K. S., Kidd, G. J., Carson, J. H., and Smith, R. (1998). hnRNP A2 selectively binds the cytoplasmic transport sequence of myelin basic protein mRNA. Biochemistry *37*, 7021–7029.

Huang, Y. S., Carson, J. H., Barbarese, E., and Richter, J. D. (2003). Facilitation of dendritic mRNA transport by CPEB. Genes Dev. *17*, 638–653.

Kobayashi, H., Yamamoto, S., Maruo, T., and Murakami, F. (2005). Identification of a *cis*-acting element required for dendritic targeting of activity-regulated cytoskeleton-associated protein mRNA. Eur. J. Neurosci. *22*, 2977–2984.

Kosturko, L. D., Maggipinto, M. J., D'Sa, C., Carson, J. H., and Barbarese, E. (2005). The microtubule-associated protein tumor overexpressed gene binds to the RNA trafficking protein heterogeneous nuclear ribonucleoprotein A2. Mol. Biol. Cell *16*, 1938–1947.

Kosturko, L. D., Maggipinto, M. J., Korza, G., Lee, J. W., Carson, J. H., and Barbarese, E. (2006). Heterogeneous nuclear ribonucleoprotein (hnRNP) E1 binds to hnRNP A2 and inhibits translation of A2 response element mRNAs. Mol. Biol. Cell *17*, 3521–3533.

Lein, E. S. *et al*. (2007). Genome-wide atlas of gene expression in the adult mouse brain. Nature *445*, 168–176.

Ling, D.S.F., Bernardo, L. S., and Sacktor, T. C. (2006). Protein kinase Mζ enhances excitatory synaptic transmission by increasing the number of active postsynaptic AMPA receptors. Hippocampus *16*, 443–452.

Lisman, J., Schulman, H., and Cline, H. (2002). The molecular basis of CaMKII function in synaptic and behavioural memory. Nat. Rev. Neurosci. *3*, 175–190.

Lyford, G. L., Yamagata, K., Kaufmann, W. E., Barnes, C. A., Sanders, L. K., Copeland, N. G., Gilbert, D. J., Jenkins, N. A., Lanahan, A. A., and Worley, P. F. (1995). Arc, a growth factor and activity-regulated gene, encodes a novel cytoskeleton-associated protein that is enriched in neuronal dendrites. Neuron *14*, 433–445.

Mayford, M., Baranes, D., Podsypanina, K., and Kandel, E. R. (1996). The 3′-untranslated region of CaMKII alpha is a cis-acting signal for the localization and translation of mRNA in dendrites. Proc. Natl. Acad. Sci. USA *93*, 13250–13255.

Miller, S., Yasuda, M., Coats, J. K., Jones, Y., Martone, M. E., and Mayford, M. (2002). Disruption of dendritic translation of CaMKIIalpha impairs stabilization of synaptic plasticity and memory consolidation. Neuron *36*, 507–519.

Mori, Y., Imaizumi, K., Katayama, T., Yoneda, T., and Tohyama, M. (2000). Two cis-acting elements in the 3′ untranslated region of alpha-CaMKII regulate its dendritic targeting. Nat. Neurosci. *3*, 1079–1084.

Mouland, A. J. *et al*. (2001). RNA trafficking signals in human immunodeficiency virus type 1. Mol. Cell. Biol. *21*, 2133–2143.

Munro, T. P., Magee, R. J., Kidd, G. J., Carson, J. H., Barbarese, E., Smith, L. M., and Smith, R. (1999). Mutational analysis of a heterogeneous nuclear ribonucleoprotein A2 response element for RNA trafficking. J. Biol. Chem. *274*, 34389–34395.

Muslimov, I. A., Nimmrich, V., Hernandez, A. I., Tcherepanov, A., Sacktor, T. C., and Tiedge, H. (2004). Dendritic transport and localization of protein kinase Mzeta mRNA: implications for molecular memory consolidation. J. Biol. Chem. *279*, 52613–52622.

Muslimov, I. A., Iacoangeli, A., Brosius, J., and Tiedge, H. (2006). Spatial codes in dendritic BC1 RNA. J. Cell Biol. *175*, 427–439.

Nichols R. C., Wang, X. W., Tang, J., Hamilton, B. J., High, F. A., Herschman, H. R., and Rigby, WFC (2000) The RGG domain in hnRNP A2 affects subcellular localization. Exp. Cell Res. *256*, 522–532.

Rial Verde, E. M., Lee-Osbourne, J., Worley, P. F., Malinow, R., and Cline, H. T. (2006). Increased expression of the immediate-early gene arc/arg3.1 reduces AMPA receptor-mediated synaptic transmission. Neuron *52*, 461–474.

Rongo, C. (2002). A fresh look at the role of CaMKII in hippocampal synaptic plasticity and memory. Bioessays *24*, 223–233.

Shan, J., Moran-Jones, K., Munro, T. P., Kidd, G. J., Winzor, D. J., Hoek, K. S., and Smith, R. (2000). Binding of an RNA trafficking response element to heterogeneous nuclear ribonucleoproteins A1 and A2. J. Biol. Chem. *275*, 38286–38295.

Shan, J., Munro, T. P., Barbarese, E., Carson, J. H., and Smith, R. (2003). A molecular mechanism for mRNA trafficking in neuronal dendrites. J. Neurosci. *23*, 8859–8866.

Shepherd, J. D., Rumbaugh, G., Wu, J., Chowdhury, S., Plath, N., Kuhl, D., Huganir, R. L., and Worley, P. F. (2006). Arc/Arg3.1 mediates homeostatic synaptic scaling of AMPA receptors. Neuron *52*, 475–484.

Tiruchinapalli, D. M., Oleynikov, Y., Kelic, S., Shenoy, S. M., Hartley, A., Stanton, P. K., Singer, R. H., and Bassell, G. J. (2003). Activity-dependent trafficking and dynamic localization of zipcode binding protein 1 and beta-actin mRNA in dendrites and spines of hippocampal neurons. J. Neurosci. *23*, 3251–3261.

Zhabotinsky, A. M., Camp, R. N., Epstein, I. R., and Lisman, J. E. (2006). Role of neurogranin concentrated in spines in the induction of long-term potentiation. J. Neurosci. *26*, 7337–7347.